A common deep source for upper-mantle upwellings below the Ibero-western Maghreb region from teleseismic *P*-wave travel-time tomography

Corresponding author's email address: cciviero@fc.ul.pt

Chiara Civiero[1], Vincent Strak[1,2], Susana Custódio[1], Graça Silveira[1,3], Nicholas Rawlinson[4], Pierre Arroucau[5], Carlos Corela[1]

1) Instituto Dom Luiz (IDL), Faculdade de Ciências, Universidade de Lisboa, Lisboa 1749-016, Portugal

2) Department of Earth Sciences, Vrije Universiteit Amsterdam, Amsterdam 1081 HV, Netherlands

3) Instituto Superior de Engenharia de Lisboa, Lisboa 1959-007, Portugal

4) Bullard Laboratories, Department of Earth Sciences, University of Cambridge, Cambridge CB30EZ, UK

5) Dublin Institute for Advanced Studies (DIAS), Dublin D02 Y006, Ireland

Abstract

Upper-mantle upwellings are often invoked as the cause of Cenozoic volcanism in the Ibero-western Maghreb region. However, their nature, geometry and origin are unclear. This study takes advantage of dense seismic networks, which cover an area extending from the Pyrenees in the north to the Canaries in the south, to provide a new high-resolution *P*-wave velocity model of the upper-mantle and topmost lower-mantle structure. Our images show three subvertical upper-mantle upwellings below the Canaries, the Atlas Ranges and the Gibraltar Arc, which appear to be rooted beneath the upper-mantle transition zone (*MTZ*). Two other mantle upwellings beneath the eastern Rif and eastern Betics surround the Gibraltar subduction zone. We propose a new geodynamic model in which narrow upper-mantle upwellings below the Canaries, the Atlas Ranges and the Gibraltar Arc rise from a laterally-propagating layer of material below the *MTZ*, which in turn is fed by a common deep source below the Canaries. In the Gibraltar region, the deeply rooted upwelling interacts with the Gibraltar slab. Quasi-toroidal flow driven by slab rollback induces the hot mantle material to flow around the slab, creating the two low-velocity anomalies below the eastern Betics and eastern Rif. Our results suggest that the Central Atlantic plume is a likely source of hot mantle material for upper-mantle upwellings in the Ibero-western Maghreb region.

1. Introduction

Cenozoic volcanism within the Ibero-western Maghreb region, an area located between the western Mediterranean Sea and the central-eastern Atlantic Ocean (Fig. 1), results from the interplay between mantle dynamics and the complex geodynamic evolution of the area (Lustrino and Wilson, 2007, and references therein). This volcanism has been attributed to both passive and active mantle upwelling processes (e.g., Duggen et al., 2004; Maury et al., 2000; Oyarzun et al., 1997; Sun et al., 2014; Teixell et al., 2005). However, no general agreement on what triggers these mantle upwellings has yet emerged.

Global seismic models (e.g., Bijwaard et al., 1998; French and Romanowicz, 2015; Li et al., 2008; Schaeffer and Lebedev, 2013; Simmons et al., 2012; Tesoniero et al., 2015; Van Der Hilst et al., 1997) provide convincing evidence of low-velocity anomalies in the upper mantle below central-eastern Atlantic, north-western Africa and southern Iberia. These low-velocity anomalies contrast with the high-velocity anomalies imaged below the Alboran Sea and central Iberia. However, global seismic models tend to resolve only broad-scale features, in part due to the non-uniform distribution of seismometers and earthquakes on Earth.

Over the past 30 years a large number of permanent and temporary regional seismic networks were deployed in Iberia, Gulf of Cadiz, Morocco and Canaries. These seismic networks have provided detailed images of upper-mantle structure, namely through body-wave travel-time tomography (e.g., Bezada et al., 2013; Bonnin et al., 2014; Koulakov et al., 2009; Monna et al., 2013; Piromallo and Morelli, 2003; Spakman et al., 1993; Villaseñor et al., 2015), surface-wave tomography (e.g., Boschi et al., 2004; Palomeras et al., 2014, 2017; Schivardi and Morelli, 2009; Villaseñor et al., 2001) and full-waveform tomography (e.g., Fichtner et al., 2013; Zhu et al., 2015). The resulting models systematically recognize an upper-mantle signature of the Gibraltar Arc System, composed of the Betic-Rif orogen, the Gibraltar subduction zone and the extensional back-arc domain of the Alboran basin (Gutscher et al., 2002) (Fig. 1). In particular, a prominent high-velocity body is clearly imaged in the upper mantle below the Alboran Sea, which is interpreted with broad consensus as a subducted lithospheric slab (Bezada et al., 2013; Bonnin et al., 2014; Palomeras et al., 2014, 2017; Piromallo and Morelli, 2003; Villaseñor et al., 2015; Wortel and Spakman, 2000).

In contrast, there is no agreement on the origin of the low-velocity mantle anomalies imaged beneath the Gibraltar Arc and Morocco regions. Below the Atlas Ranges, the observed low-velocity anomalies, thinned lithosphere (~60 km) and uplifted topography (Ayarza et al., 2014; Fullea et al., 2010; Missenard et al., 2006; Palomeras et al., 2014; Teixell et al., 2005; Zeyen et al., 2005) have been attributed to: 1) Edge-driven convection, where a large step in lithospheric thickness between the thicker western African Craton and the thinner Atlas Mountains triggers mantle upwelling and subsequent decompression melting (Fullea et al., 2010; Kaislaniemi and Van Hunen, 2014; Missenard and Cadoux, 2012; Ramdani, 1998); 2) delamination of an unstable lithospheric mantle (Bezada et al., 2014; Duggen et al., 2009; Levander et al., 2014); 3) impingement of a small plume rising from a deep source directly below Morocco (Teixell et al., 2005; Zeyen et al., 2005); and 4) inflow of Canary mantle-plume material in the topmost upper mantle (Duggen et al., 2009; Hoernle et al., 1995; Mériaux et al., 2015a; Miller and Becker, 2014; Oyarzun et al., 1997). The less studied low-velocity anomalies found below the eastern Rif and eastern Betics, on both sides of the Gibraltar subduction zone, have been associated with: 1) Edge-driven convection below the eastern Rif associated with a step in lithospheric thickness (Kaislaniemi and Van Hunen, 2014); and 2) tearing of the lithosphere below the Betics (Pérez-Valera et al., 2013) or below both the Betics and the Rif (Frizon de Lamotte et al., 2009; Levander et al., 2014; Palomeras et al., 2014; Thurner et al., 2014), with upwelling material replacing the lithosphere at the tear location.

The Canary archipelago is an oceanic intraplate hotspot (Morgan, 1972), located ~100 km off the north-west coast of Africa. Although the Canaries have been extensively studied using seismic methods (Bonnin et al., 2014; Lodge et al., 2012; Martinez-Arevalo et al., 2013; Miller et al., 2015; Montelli et al., 2006; van der Meijde et al., 2003), the origin of its underlying anomalous low-velocity mantle is still debated. Global seismic models feature low

P-wave velocities suggesting a ~400 km wide mantle plume that extends down into the lowermost mantle (Montelli et al., 2006, 2004; Zhao, 2004). However, the lack of a regional high-resolution tomographic model prevents the imaging of the true lateral extent and vertical continuity of the plume-like anomaly.

In this article, we extend previous body-wave studies (Bezada et al., 2013; Bonnin et al., 2014; Chevrot et al., 2014; Monna et al., 2013) by combining data from dense permanent and temporary seismic networks in Iberia, northern Morocco, Canaries and Gulf of Cadiz (Fig. 2). The combined dataset allows the computation of a high-resolution *P*-wave travel-time tomographic model, which extends from ~50 to 800 km depth and resolves new details of the mantle seismic structure (Fig. S1 and S2). Compared to previous models, two important improvements are: 1) A larger number of combined onshore and offshore (*OBS)* stations (~25% more than those used in Bezada et al., 2013) with a more uniform distribution, in particular in Western Iberia (29 more stations compared to what is used in Bezada et al., 2013), Gulf of Cadiz and Canaries (28 and 9 more stations respectively in comparison to the arrays used in Bezada et al., 2013 and Villaseñor et al., 2015), translating into improved structural recovery, particularly in the *MTZ*; and 2) the introduction of a *3D* starting model (*PRISM3D*) inferred from previous seismic studies (Arroucau et al., 2017). *PRISM3D* includes detailed crustal and Moho structure, which will improve the robustness of the mantle model by minimizing the contributions to the travel-time anomalies from unresolved crustal structure. The resulting tomographic model allows the investigation of the degree of connection between upper-mantle and topmost lower-mantle features, and implications for the origin of upper-mantle upwellings in the Ibero-western Maghreb region. Motivated by our tomographic model, we propose a new geodynamic model to explain upper-mantle upwellings in the region, consistent with previous global tomographic models, numerical and analogue modelling, geochemical observations and surface volcanism.

2. Dataset and method

2.1. Dataset

We combined broadband teleseismic *P*-wave travel-time data, recorded between 2007 and 2013, from 18 seismic networks in the Ibero-western Maghreb region. About 200 seismometers were deployed in Spain and Morocco between 2007 and 2013 by the IberArray experiment (Díaz et al., 2009). Overlapping in space and time with IberArray, 64 broadband seismometers from the PICASSO project operated in Morocco and part of Spain between 2009 and 2013 (Platt et al., 2008). An additional 23 temporary seismic stations operated in mainland Portugal between 2010 and 2012 as part of the WILAS project (Custódio et al., 2014). We further used data from 24 temporary broadband *OBS*s deployed by the NEAREST experiment between 2007 and 2008 (Carrara and NEAREST Team, 2008). Data from 5 additional broadband *OBS*s of the TOPOMED project, recorded between 2009 and 2010, were also included (Grevemeyer, 2011). Finally, data from 100 permanent and temporary stations from 13 other seismic networks in Spain, Portugal, Morocco, France and Canaries, which operated throughout the period of analysis, were exploited in this study. Data from a total of 416 seismic stations were used in this work (Fig. 2). Station information can be found in the Supplemental Information Tables ST1 and ST2. This dataset extends the areal coverage significantly further than previous investigations. A noteworthy consequence of the improved coverage is an increase in the density of crossing rays within the *MTZ* (Fig. S3), thus allowing the interpretation of the seismic velocity structure down to the uppermost lower mantle with confidence.

We analysed *P*-waves generated by 451 teleseismic events, with magnitudes mb ≥ 5.5, in the teleseismic epicentral distance range $30° < \Delta < 95°$, and with sufficient signal-to-noise ratio to allow the extraction of reliable arrival-times. Figure 2 shows the relatively uniform distribution of earthquakes with respect to the centre of the study area.

All traces were first aligned using travel-time predictions from the *ak*135 global reference model (Kennett et al., 1995) and low-pass filtered at 5 Hz. The adaptive stacking technique of Rawlinson and Kennett, (2004) was then used to align the traces of each phase to obtain relative arrival-time residuals, which reflect variations in wavespeed beneath the stations. We also analysed the pattern of travel-time residuals as a function of source location in order to minimise the presence of spurious arrivals. Supplemental Figure S4 shows the back-azimuthal variation of the travel-time residuals for stations located in different zones of the Ibero-western Maghreb region. Our final dataset is composed of 25644 relative *P*-wave travel-times.

2.2. Inversion procedure

We used the *FMTOMO* package in order to generate a tomographic model for the Ibero-western Maghreb region from the teleseismic dataset (de Kool et al., 2006; Rawlinson et al., 2010; Rawlinson and Urvoy, 2006). *FMTOMO* solves the forward problem of travel-time prediction using the Fast Marching Method (*FMM*), a grid-based eikonal solver (de Kool et al., 2006; Rawlinson and Sambridge, 2004; Sethian, 1996). Model parameters are adjusted with a subspace inversion technique (Kennett et al., 1988). The forward and inverse steps are applied iteratively in order to address the weakly non-linear nature of the inverse problem. *FMTOMO* allows the recovery of *3D* velocity variations, interface depth, and source location. However, in our application we invert only for perturbations to the *3D* mantle *P*-wavespeed.

The study region was discretized into a total of 74152 velocity grid nodes: 52 nodes in latitude (26°-46°N); 62 nodes in longitude (19°W-5°E); and 23 vertical nodes, extending from the Moho down to 800 km depth. This corresponds to a node spacing of 0.4° horizontally in both latitude and longitude, and ~35 km in depth. The velocity grid values represent unknowns in the inversion, and are used to control a smooth velocity continuum defined by a regular mosaic of cubic *B*-spline functions. We follow the procedure of Rawlinson et al., (2006) to evaluate the trade-off between fitting the data and satisfying regularization constraints. The resulting trade-off curve shows that a damping value of $\varepsilon = 5$ and a smoothing value of $\eta = 5$ provide a good compromise between variance reduction and roughness of the solution (Fig. S5). The final model reduces the data variance by 53%, from 0.41 s^2 to 0.19 s^2.

One of the recognised weaknesses of teleseismic tomography is that shallow structure, down to a depth approximately equal to the station spacing, is poorly constrained (e.g., Rawlinson et al., 2010). We address this problem by including an *a priori 3D* crust and Moho model (*PRISM3D*) in our starting model, which has the effect of correcting for unresolved crustal contributions to the measured arrival-time residuals (Arroucau et al., 2017). *PRISM3D* also includes a *3D* absolute *P*-wave velocity model of the upper mantle beneath the Ibero-western Maghreb region, which is based on a number of different data sources. It was primarily designed for earthquake source studies but also provides a useful *a priori* model for local and teleseismic tomography. Details of the *PRISM3D* model are given in the Supplemental Information (SA1 and Fig. S6).

Figure 3 shows three depth slices, at 20 km, 400 km and 700 km, through the starting model down to the base of the *MTZ*. The initial velocities in the topmost lower mantle (660-800 km depth) are those from the *LLNL* global *P*-wave tomographic model of Simmons et al., (2012), which was built from approximately 3 million *P*- and *Pn*- arrivals. Velocity perturbations are shown relative to a depth-dependent *1D* lateral average of our initial model (Fig. 3d).

The joint use of relative travel-time residuals from multiple arrays operating at different time periods may result in the loss of long-wavelength features (Rawlinson et al., 2014). However, the inclusion of the broad-scale initial models *PRISM3D* and *LLNL*, where the longer wavelength information is preserved, mitigates this issue by providing reasonably accurate background velocities beneath the arrays. Further verification of this approach can be found in Rawlinson and Fishwick, (2012) and Rawlinson et al., (2014).

3. Resolution tests

We analyse the resolving power of our dataset via synthetic tests. The synthetic dataset is obtained by solving the forward problem in the presence of a known Earth structure with prescribed velocity variations and using the same sources, receivers and phase types as the field dataset. Gaussian random noise with a standard deviation of 0.1s, which is similar to the noise level in the true dataset, is added to the synthetic data. The inversion scheme is then applied to the synthetic dataset, using the same damping and smoothing parameters used for the inversion of real data.

We carry out two standard checkerboard tests, where positive and negative velocity anomalies, with amplitudes of ± 0.50 km/s and diameters of ~140–200 km, are superimposed on the starting model. The comparison between input and output models suggests a good lateral resolution for features of 140 km diameter in the upper mantle below most of the study area, excluding the north-western Atlantic Ocean and Algeria (Fig. 4c, d). Some horizontal smearing occurs in the topmost lower mantle, at the edges of the broad network, but we can still recover features with diameters of the order of ~200 km (Fig. S7d). For anomalies of this size, vertical resolution is good down to the bottom of the model, although smearing at the edges of the domain tends to blur the recovered structure. We mark the limits of the well-resolved structure by comparing input and output synthetic models, using the ~200 km anomalies, at various depths (Fig. S7). Later, when interpreting the model, we use these same limits to delineate the robust regions of the model.

We also perform a structural resolution test (Fig. 5) where we place three vertical slow structures (δV_P = -0.50 km/s) in the upper mantle below the Canaries, the Atlas Ranges and the Gibraltar Arc and three separated horizontal slow layers below the *MTZ*. The recovered images (Fig. 5c, e, g) can be used to evaluate the connectivity of each of the vertical and horizontal pairs of anomalies. While low-level smearing which connects the two anomalies can be observed in each case, the separate input anomalies can nonetheless be clearly identified, particularly those restricted to the upper mantle. This helps to confirm that if a separation between the upper- and lower-mantle features did actually occur, it would have been recovered in the inversion.

We also carry out two sets of discrete spike tests (anomalies of δV_P = -0.50 km/s, diameter = ~100 km), to examine whether (i) features in the *MTZ* can be recovered independently of those in the upper mantle and lower mantle (Fig S8), and (ii) deep upper mantle structure can be recovered independently from shallow upper-mantle structure below the Canaries (Fig. S9). In both cases, our test results confirm that smearing does not compromise either of these two scenarios.

A final resolution test (Fig. S10) is carried out to investigate a proposed sub-lithospheric channel connecting the Canaries and the Atlas low-velocity anomalies (e.g., Duggen et al., 2009). In this test, the sub-lithospheric channel is modelled as a narrow, shallow low-velocity anomaly (~150 km width, between ~50 and 150 km depth, δV_P = 0.5 km/s). The output model recovers almost the entire extent of the input low-velocity corridor. If such a corridor exists, we expect it to be well resolved in our model. In this scenario, the only region that cannot be well resolved is a narrow area below the western Moroccan coast (Fig. S10b).

4. Tomographic model

Figure 6 shows depth slices, ranging between 70 km and 730 km, through the *P*-wave tomographic model. Figure 7 shows cross-sections that depict what we regard as the most significant anomalies. In addition, we compute two more inversions with different mantle starting model, one with the ak*135* spherically symmetric Earth model (Kennett et al., 1995) (Fig. S11) and the other with the *LLNL 3D* global model (Simmons et al., 2012) (Fig. S12). All other initial parameters are otherwise identical, including the Moho interface and crustal structure. These tests demonstrate that the primary structures imaged are not dependent on the use of the *PRISM3D* mantle model as a starting model. We focus on the interpretation of the model that uses the *PRISM3D* starting model in the mantle because it mitigates the issue of using multiple arrays recording at different times and it contains smaller-scale structure than the *LLNL* model.

Because we use relative arrival-time residuals as inputs to our tomographic inversion, the output velocity anomalies are also relative. An important question when interpreting the anomalies is whether they are truly representative of fast and slow material, or whether, for example, low-velocity anomalies represent normal or average wavespeeds, but are slow in comparison to very fast anomalies (although if we assume that our longer wavelength *3D* starting model is robust, then this scenario is less likely). Another recent hypothesis proposes that low-velocity features surrounding fast anomalies, like slabs, may be an artefact introduced to isotropic models when anisotropic effects are not accounted for during the inversion (Bezada et al., 2016). Previous studies have already recognized on a global scale that the Alboran Sea region is particularly fast at upper-mantle depths and that the structure surrounding it is generally slow (e.g., Li et al., 2008; Ritsema et al., 2011; Simmons et al., 2012, 2010). Recent regional surface-wave analysis revealed fast absolute shear-wave velocities of ~4.6 km/s below the Alboran Sea and slow velocities of 4.1-4.4 km/s below the Betics, Strait of Gibraltar, Rif and northern African margin, in the 100-200 km depth range (Palomeras et al., 2014). In addition, synthetic tests done in previous body-wave tomographic studies (Bezada et al., 2014) showed that the artificial ring of low velocities expected around the fast slab as a result of relative travel-time tomography is much thinner and smaller in amplitude than the actual low-velocity anomalies that are imaged. Although additional inversions which take into account upper-mantle anisotropy may help to better define the extent of the low-velocity anomalies, all these observations suggest that the low-velocity anomalies in the region are likely real.

4.1. Low-velocity anomalies

Our tomographic model includes several well-resolved velocity anomalies (Fig. 6). A low-velocity anomaly is imaged below the western Canaries (*L1*, $\delta V_P \approx -0.1$ km/s), narrow at shallow depths (~130 km depth, Fig. 6b) and which progressively broadens down and eastward to 550 km depth (Fig. 6i). *L1* remains visible at deeper levels and spreads broadly beneath the *MTZ* (Fig. 6k, l; Fig. 7d, g).

L2 is a broad slow anomaly, with a diameter of ~150-250 km, which extends throughout the upper mantle below Morocco. The areal extent of *L2* coincides with the Middle and High-Atlas Mountains. This slow anomaly has been identified in previous tomographic studies (e.g., Bezada et al., 2014; Bonnin et al., 2014; Palomeras et al., 2014; Villaseñor et al., 2015). Our model can now resolve its connection to the lower mantle, showing that *L2* extends through the *MTZ*, and seemingly connects to *L1* below ~600 km depth (Fig. 6g-l; Fig. 7d, g). The magnitude of *L2* decreases with depth from $\delta V_P \approx -0.3$ km/s in the upper mantle to about −0.1 km/s in the topmost lower mantle.

Another clear low-velocity anomaly is *L3* located below the Gibraltar Arc (~200 km diameter, δV_P ranging from ~-0.1 to below ~-0.3 km/s). Again, this anomaly has also been found in previous studies (Bezada et al., 2013; Bonnin et al., 2014; Monna et al., 2013). Similar to *L2*, *L3* penetrates down to the lower mantle, merging with *L1* below the *MTZ* under the western African margin (Fig. 6k, l).

A prominent low-velocity anomaly ($\delta V_P \approx -0.2$ km/s) beneath the eastern Rif, *L4* , appears to be restricted to the upper mantle (Fig. 6b-g; Fig. 7b, c). Another low-velocity feature is *L5*, located below the eastern Betics, coinciding with the Calatrava and Cofrentes Province and with a δV_P ranging from ~-0.1 to below ~-0.3 km/s (Fig. 6b-g; Fig. 7b, e).

Adjacent to *L5,* a small-scale low-velocity body is imaged beneath the Valencia Trough (*L6,* $\delta V_P \approx -0.1$ km/s), corresponding to the area offshore north and northeast of the Balearic Islands (Fig. 6; Fig. 7f).

4.2. High-velocity anomalies

The most conspicuous fast body in the region is anomaly *H1* ($\delta V_P > 0.3$ km/s at its centre), located below the Alboran Sea, Betics and internal Rif. In some places, this body extends from the surface down to the *MTZ* (Fig. 6; Fig. 7a-c). *H1* is arcuate in shape, concave on the Alboran Sea side down to ~400 km depth and dips steeply downward. This structure has been studied extensively since the late 1980s (e.g., Bezada et al., 2013; Blanco and Spakman, 1993; Duggen et al., 2004; Gutscher et al., 2002; Hoernle et al., 1999; Torres-Roldan et al., 1986) and is interpreted as lithospheric material subducted during the closure of the Mediterranean Sea.

A smaller blob-like high-velocity feature, *H2*, is imaged in the Atlantic Ocean, west of the Strait of Gibraltar, below the Gorringe Bank. It has a diameter of ~350 km and dips slightly eastward down to a depth of at least 300 km (Fig., 6; Fig. 7a, e). The magnitude of *H2* decreases with depth from $\delta V_P \approx 0.2$ km/s near the surface to 0.1 km/s above the *MTZ*. This result is qualitatively consistent with that obtained from the body-wave study of Monna et al., (2013).

We also identify several other positive velocity anomalies; however, they are not integral to our interpretation, and therefore will not be discussed at length. A prominent high-velocity anomaly ($\delta V_P \approx 0.1$-0.2 km/s) is imaged below Western Iberia (*H3*), down to the topmost lower mantle (Fig. 6; Fig. 7f). Although few efforts have been made to interpret it, *H3* has already been imaged in previous tomographic studies (Bonnin et al., 2014; Monna et al., 2013; Villaseñor et al., 2015). Monna et al., (2013) associate *H3* to the sinking of colder oceanic lithosphere. South of the Pyrenees, we observe a high-velocity body with an elongated *NW-SE* shape ($\delta V_P = \sim 0.1$-0.2 km/s), *H4*, which seems to extend across the *MTZ* (Fig. 6). This feature is consistent with that imaged previously by Souriau et al., (2008) and Chevrot et al., (2014). In Morocco, we locate a high-velocity body below the Moroccan Meseta (*H5,* $\delta V_P = \sim 0.1$-0.3 km/s) and beneath the Anti Atlas (*H6,* $\delta V_P = \sim 0.1$-0.2 km/s) (Fig. 6), both of which have been recovered in previous regional tomographic studies (e.g., Bezada et al., 2014; Bonnin et al., 2014; Villaseñor et al., 2015). It is worth noting, however, that the inversion method used here resolves relative velocity perturbations, which are tied to absolute velocities through the starting *3D* model *PRISM3D*. Thus, if *PRISM3D* is too fast in the neighbourhood of *H3* for example (which sits below the WILAS array), it will likely also be too fast in the final model. Also, since we show the anomalies relative to a *1D* laterally averaged depth-dependent version of *PRISM3D*, a small variation in the background model may result in slow anomalies being even slower and fast anomalies becoming less fast than those presented in our model (Bastow, 2012) (see Fig. S13).

5. Discussion

In this section, we use our seismic model to discuss the dynamics of the upper mantle and topmost lower mantle in the Ibero-western Maghreb region. We focus on the multiple upper-mantle low-velocity anomalies observed below the Canaries, Atlas Ranges, Gibraltar Arc, eastern Betics and eastern Rif. We question the role of the lower mantle in the apparent ascent of material and we discuss the possible interaction of upwellings with the high-velocity body of the Alboran domain.

5.1. Roots of upper-mantle upwellings

As presented in Section 1, different geodynamic processes have been proposed to explain the consistently imaged low-velocity seismic anomalies below the Ibero-western Maghreb region. Albeit different in their details, all processes invoke mantle upwellings, with different signatures in terms of size, extent and depth of seismic anomalies. The anomalies identified in our model confirm the widespread presence of upper-mantle upwellings in the study region. In particular, anomalies *L1*, *L2* and *L3* appear as 'finger-like' conduits, connected to a broader low-velocity body in the topmost lower mantle in the Atlantic Ocean (Fig. 6 and 7). Our tomographic images of *L1* are in good agreement with previous research that suggests a deep mantle plume below the Canaries (Anguita and Hernán, 2000; Montelli et al., 2006; Zhao, 2007), which we will refer to as the Central Atlantic mantle plume. Two previous receiver function studies (Martinez-Arevalo et al., 2013; Miller et al., 2015) found a low-velocity layer in the shallow upper mantle (just below the lithosphere at ~45-100 km depth) beneath the Canaries, which does not extend deeper into the upper mantle. In our results, we instead observe a vertical low velocity anomaly extending to the *MTZ*, which resolution tests (see Fig. S9) indicate is unlikely to be the result of shallow structure smeared at depth. Although some ponding of material may exist at 45-100 km depth, our model clearly images a sub-vertical connection to lower depths. Additional stations deployed both inboard and outboard of the African coast would of course improve the recovery of anomaly *L1*. Anomaly *L2* – as imaged in our model – is hard to reconcile with edge-driven convection and lithospheric delamination models, which are expected to form shallow anomalies confined to the topmost upper mantle (e.g., Bezada et al., 2014; Missenard and Cadoux, 2012) rather than anomalies extending down to the lower mantle. Nevertheless, we do not exclude that edge-driven convection and lithospheric delamination may occur below the Atlas Ranges. Rather, we question their ability to produce detectable low-velocity anomalies below the lithosphere. Indeed, both processes can generate topmost upper-mantle upwellings of smaller scale than that resolved by our model, without necessarily sourcing abnormally hot deep mantle material (Ballmer et al., 2015; Kaislaniemi and Van Hunen, 2014). One possible explanation that reconciles these different views is that smaller-scale edge-driven convection and lithospheric delamination may be superimposed on the larger-scale deeply-rooted upwelling. In support of the latter process, a few small-scale high-velocity anomalies are present in our results (see Fig. 6e,f), similarly to what was found by Bezada et al., (2014), which they interpreted as delaminated lithosphere sinking into the upper mantle. To the best of our knowledge, no explanation has yet been proposed for anomaly *L3*, which has also been previously imaged at upper-mantle depths (e.g., Bonnin et al., 2014; Monna et al., 2013).

Is the slow upper-mantle structure beneath Morocco and the Gibraltar Arc System connected with material coming from the Central Atlantic mantle plume? A previously suggested hypothesis proposed the channelling of material from the Central Atlantic mantle plume head, through the north-west African sublithospheric corridor, to the mantle wedge of the Gibraltar subduction zone (e.g., Duggen et al., 2009; Mériaux et al., 2015a). Upward flow along the base of the lithosphere, possibly assisted by edge-driven convection and/or lithospheric delamination, could then have contributed to Cenozoic volcanism along the lithospheric corridor (Duggen et al., 2009). In spite of the weaker resolution of our model in the oceanic domain, between the Canaries and the western Moroccan coast, our tomographic images show a clear disconnection between anomalies *L1* and *L2* at shallow upper-mantle depths (Fig. 6a-d; Fig. 7d; Fig. S10). This result, supported by the absence of a single continuous thinned area under the Atlas Mountains (Fullea et al., 2010), casts doubt over the existence of a sublithospheric corridor allowing material to flow northeastwards from the Central Atlantic mantle plume. An alternative geodynamic model suggested by Miller et al., (2015) invokes the presence of an upper-mantle plume composed of a main sub-vertical branch below the Canaries from which another highly tilted branch towards the Atlas Ranges emerges. This model also suggests that the Canary plume is a common origin for upper-mantle upwellings below the Atlas Ranges and the Rif Mountains. We note, however, that this model requires the existence of an eastward background mantle flow. Moreover, it lacks resolution within and below the *MTZ* and consequently, provides no interpretation of the deeper structure.

Instead of the above models, we propose a scenario in which the upper-mantle upwellings *L1*, *L2* and *L3* originate from hot material ponded at the very top of the lower mantle, below the 660-km mantle discontinuity (or '660'). This endothermic phase transition is expected to resist upward flow, opposing the penetration of lower-mantle material into the upper mantle. In some places, such as the Canaries, the Atlas Ranges and the Gibraltar Arc, thermal instabilities seem to have successfully developed into 'secondary' mantle upwellings, which cross the *MTZ* and rise into the upper mantle (Cserepes and Yuen, 2000; Tosi and Yuen, 2011). Our tomographic model suggests that material below the *MTZ* spreads laterally from below the Canaries to the Atlas Ranges and the Gibraltar Arc (see Fig. 6k-l; Fig. 7d, e, g). The ponded material has a geographical overlap with the northern area of the Central Atlantic Hotspot Province (*CAP*), which spans from the central-eastern Atlantic near the Canary-Cape Verde hotspots to north-western Africa. It has been suggested that the *CAP* has been fed by a broad plume since at least 90-100 Ma (Oyarzun et al., 1997).

Tomographic (e.g., Boschi et al., 2007; Montelli et al., 2004) and analogue (Davaille et al., 2005) models are consistent with a mantle plume originating at the core-mantle boundary below the *CAP,* and stalling at the *MTZ*, and secondary upper-mantle upwellings rising below the Canary hotspot (in addition to Cape Verde, Great Meteor and Azores, which are outside of our study region). Geochemical analyses of Tertiary-Quaternary alkaline basalts from the central-eastern Atlantic and western Mediterranean suggest a unique long-lived reservoir with a typical *OIB-HIMU* signature below the entire area (e.g., Hoernle et al., 1995; Lustrino and Wilson, 2007; Piromallo et al., 2008). Below the Canaries, the *HIMU* component appears to have its clearest fingerprint, whereas it becomes more diluted by a sub-lithospheric component (Bell et al., 2004; Cadoux et al., 2007; Hoernle et al., 1995; Lustrino and Wilson, 2007; Wilson and Downes, 1991) or mixed with shallower depleted astenospheric reservoirs (e.g., Gasperini et al., 2002) moving northeast towards Morocco, Iberia and Central Europe. Receiver-function (e.g., Bonatto et al., 2015; Lawrence and Shearer, 2006; Spieker et al., 2014) and *PP*/*SS* precursor (e.g., Deuss, 2007; Houser et al., 2008; Saki et al., 2015) analyses found a significant *MTZ* thinning below the low-velocity anomalies identified in our study area, namely in the Canaries (~240 km), Atlas Ranges (~240 km) and Gibraltar Arc (~220-240 km). However, some contradictory results have been obtained below the Atlas Ranges. While the 410 km discontinuity has been found overall to be deeper than average, some discrepancies exist for the topography of the '660'. Below the Western Atlas, Bonatto et al., (2015) found a slightly elevated '660'. In contrast, the study of Spieker et al., (2014) detected no variation in depth of the '660'. However, Deuss (2007) suggested that a deeper 410km discontinuity together with an unaffected '660' might be consistent with hot upwellings rising from the lower into the upper mantle. In addition, previous studies have also suggested a mantle temperature excess of ~150-350 K below Morocco and the Gibraltar Arc (Bonatto et al., 2015; Sun et al., 2014) and ~100-400 K below the Canaries (Saki et al., 2015). These results are in agreement with a scenario of multiple hot upwellings beneath the Ibero-western Maghreb region, sourced from a hot layer ponded below the *MTZ*, which in turn is fed by the Central Atlantic mantle plume.

Our new model is also consistent with previous global tomographic studies (e.g., Kárason and van der Hilst, 2001; Simmons et al., 2012, 2010; Tesoniero et al., 2015), which image a broad low-velocity body in the lower mantle, originating at the core-mantle boundary below the *CAP* and tilting north-eastward towards the surface. However, global studies are unable to resolve the smaller-scale heterogeneities that we have retrieved in our body-wave tomography. Figure 8 shows a comparison between our regional model and the global model *LLNL* of Simmons et al., (2012). The blob-like upper-mantle slow anomalies imaged in the *LLNL* model become well-resolved multiple vertical upwellings in our model, sourced from the large-scale lower-mantle plume below the *CAP*.

Numerical models show that a lower-mantle plume with a strongly temperature-dependent rheology may be deflected horizontally just below an endothermic phase transition, where it forms a localized thermal boundary layer that can trigger smaller-scale upper-mantle upwellings (e.g., Bossmann and Van Keken, 2013; Cserepes and Yuen, 2000; Kumagai et al., 2007; Tosi and Yuen, 2011; van Keken and Gable, 1995). A sharp decrease in viscosity from the lower to the upper mantle will cause a drop in the width of the rising upwellings (100-200 km diameter for upper-mantle upwellings and 1000-2000 km diameter for lower-mantle plumes), as well as an increase in ascent rate (Kumagai et al., 2007; Leng and Gurnis, 2012; van Keken and Gable, 1995). The decrease in the width of the upwellings from the lower to the upper mantle that we infer in our model is thus to be expected from the viscosity contrast between lower and upper mantle (Fig. 8). In the lower mantle, if the viscosity contrast between plume and surrounding material is high enough, then the ponded material may flow laterally as far as ~1000 km (Tosi and Yuen, 2011).

Finally, laboratory experiments that explore the behaviour of plumes across the *MTZ* have shown that narrower upwellings can develop above a hot stagnant lower-mantle plume, with hot material ponding underneath the *MTZ* ("rebirth mode", see Kumagai et al., 2007). Analogue models predict a spacing between narrow upper-mantle upwellings of 500-1200 km (Kumagai et al., 2007), consistent with the distances that we obtain between anomalies *L1* and *L2-L3*.

5.2. Interaction with the Gibraltar slab

Our results show that *L4* and *L5* surround the retreating Gibraltar slab and are clearly connected with *L3* (Fig. 6 and 7). Their location, approximately below the basal lithospheric steps south and north of the Alboran basin (Fullea et al., 2010), makes edge-driven convection a plausible mechanism for their origin. However, as discussed in Section 5.1., if edge-driven convection were to generate low-velocity anomalies, one would expect such anomalies to be of small scale and localised under the lithospheric steps (e.g., Ballmer et al., 2015).

A hypothesis consistent with the imaged anomalies is that *L3* is deflected by mantle flow driven by the Gibraltar slab (*H1*). Numerical and laboratory subduction models (Funiciello et al., 2006; Li and Ribe, 2012; Piromallo et al., 2006; Schellart, 2008; Stegman et al., 2006; Strak and Schellart, 2014) show that a narrow rolling-back slab induces strong quasi-toroidal mantle flow around the lateral slab edges. We propose that the toroidal component of slab rollback-induced mantle flow entrained hot upwelling mantle material from the sub-slab domain (*L3*), directing hot material around the lateral slab edges to below the eastern Betics and eastern Rif. Fast polarization directions of *SKS*-waves (Buontempo et al., 2008; Díaz et al., 2015, 2010; Miller et al., 2013) show a general trend of slab rollback-induced toroidal mantle flow in the Gibraltar region. Fully dynamic models of interaction between a slab and a sub-slab mantle upwelling have shown that the quasi-toroidal mantle flow driven by the slab can transport the hot material around the lateral slab edges even before the slab comes in contact with the upwelling (Mériaux et al., 2016, 2015b). Subduction-induced quasi-toroidal mantle flow has both a lateral and an upward component (Strak and Schellart, 2014). Therefore, the interaction between deeply sourced hot upper-mantle upwelling (*L3*) and slab-induced quasi-toroidal and upward flow may explain the vigorous Cenozoic volcanism in the Betic-Rif area (Duggen et al., 2009, 2005; El Azzouzi et al., 2010; Lustrino and Wilson, 2007). In this case, the upward mantle flow induced by slab rollback would have facilitated decompression melting. The absence of recent volcanic activity may result from the very slow slab movement today (Neres et al., 2016; Serpelloni et al., 2007; Stich et al., 2006). Subduction models show that subduction velocity strongly decreases when the downdip tip of the slab reaches the *MTZ*. Our tomography model images a subvertical slab in contact with the *MTZ*, therefore we can expect a negligible present-day subduction velocity. The strong decrease in subduction velocity would naturally lead to a decrease in subduction-induced mantle flow velocity and rates of upward motion (Strak and Schellart, 2014), thereby causing the cessation of volcanism in the Betic-Rif area.

5.3. Wider geodynamic context

In agreement with previous regional studies, our tomographic model shows pervasive low-velocity anomalies in the upper mantle below the Ibero-western Maghreb region (Bezada et al., 2013; Bonnin et al., 2014; Chevrot et al., 2014; Monna et al., 2013) (Fig. S1 and S2). We find multiple upper-mantle upwellings (*L1, L2, L3*, <250 km diameter) that rise directly from the lower mantle, through the *MTZ,* below the Canaries, Atlas Ranges and Gibraltar Arc. We also identify another two upwellings (*L4*, *L5*) around the Gibraltar slab beneath the eastern Rif and eastern Betics. The material in these two anomalies may be sourced from *L3* and therefore ultimately fed by the material ponded below the *MTZ*.

The mantle heterogeneities that we image are reminiscent, in shape and geochemistry, to those found in central Europe under the French Massif Central (Granet et al., 1995) and Eifel in Germany (Ritter et al., 2001). Although the resolution is poor in the north-eastern part of our model, we note that the *L5* anomaly continues north-eastward at asthenospheric depths below the Valencia Trough (*L6*) (Fig. 6). We speculate that hot mantle material from *L5* may be guided towards the thinned Valencia Trough and through the eastern Pyrenees, connecting to mantle upwellings distributed below Central Europe, similar to the model proposed on a wider scale by Oyarzun et al. (1997). In addition, mantle upwellings *L2*, *L3* and *L5,* together with strong subduction-induced mantle flow, may connect around portions of thickened lithosphere, skirting the high-velocity bodies below the Moroccan Meseta (*H5*), Anti Atlas

(*H6*), Western Iberia (*H3*) and pieces of detached lithosphere below the Southern Pyreenes (*H4*).

Figure 9 summarises the geodynamic model that we propose for the Ibero-western Maghreb region. The simplified features do not capture all the complexity of the actual imaged structure. Nevertheless, they provide a schematic view of the mantle dynamics involved in the generation of the low-velocity anomalies discussed. A unique lower-mantle source, together with the interaction of narrower upper-mantle upwellings with upper-mantle flow induced by the sinking Gibraltar slab, is consistent with geological, seismological, and geochemical observations and explains the widespread low-velocity anomalies imaged in our model, as well as the observed surface volcanism.

Similar mechanisms invoking the connection of a deep broad plume with smaller-scale upwellings in the upper mantle, have been proposed before for the Azores, Canaries and Cape-Verde hotspots in the Atlantic ocean (Hoernle et al., 1995; Saki et al., 2015) and for East Africa below the Main African Rift and Afar (Civiero et al., 2016, 2015). The additional complexity that results from the upwelling-slab interaction has also been reported for other regions, namely for Yellowstone, where a plume may be deflected by Cascadia subduction-induced mantle flow (Kincaid et al., 2013), and for the Samoa-Tonga system, where Samoa mantle plume material flows around the northern lateral edge of the Tonga slab (Druken et al., 2014; Smith et al., 2001; Turner and Hawkesworth, 1998).

A comparison of our tomographic images with numerical models will help to conclusively establish the extent to which rollback of the Gibraltar slab has impacted active mantle upwelling in the sub-slab domain, as well as the timing and areal extent of the processes.

6. Conclusions

We combined *P*-wave arrival-time residual data from 18 experiments in the Ibero-western Maghreb region to obtain a new tomographic model, which extends from the surface down to the uppermost lower mantle. We use the velocity model *PRISM3D* as a starting model down to the base of the *MTZ* and the global model *LLNL* from the base of the *MTZ* down to a depth of 800 km.

From our results, we infer the presence of upper-mantle upwellings below the Canaries, the Atlas Ranges and the Gibraltar Arc. These upwellings are continuous from the topmost upper mantle to ~800 km depth and appear to be connected to a broad and strong low-velocity anomaly in the lower mantle. Other strong mantle upwellings are imaged around the Gibraltar slab, below the eastern Betics and eastern Rif.

The resolved structure suggests the existence of multiple upwellings in the upper mantle, with a common deep source below the Canaries, which is likely to be the Central Atlantic plume. The ascent of hot material appears to stall below the *MTZ* and then rise in the form of thinner upwellings through the upper mantle. Subduction-induced quasi-toroidal mantle flow associated with the Gibraltar slab transports deeply-sourced material from below the slab towards its lateral slab edges. Upward flow due to slab rollback may have facilitated decompression melting, thereby providing a source for Cenozoic volcanism in the Betics and Rif.

Acknowledgments

We thank two anonymous reviewers for their thoughtful reviews. The present research is supported by the Fundação para a Ciência e a Tecnologia under the Project SPIDER (PTDC/GEO-FIQ/2590/2014). We would like to thank the many scientists involved in the collection of data used in this study. Most of the data provided for this study is archived at the ORFEUS data center (https://www.orfeus-eu.org). The digital object identifier (DOI) for each network is provided in the Supplemental Information. Some instruments deployed in Portugal belong to the Portuguese national seismic network operated by IPMA (https://www.ipma.pt/). Thanks to Ingo Grevemeyer for access to data from the TOPOMED *OBS* deployment as well as Luis Matias for NEAREST *OBS* data. We thank the Instituto Geografico National (Spain) for providing us with seismic data recorded from stations deployed in Canary Islands. We thank Mitchell Liddell for his precious help with the Adaptive Stacking and FMTOMO codes. We also thank João Duarte and João Mata for their constructive comments, which helped us improve our manuscript. SAC (Helffrich et al., 2013) and GMT (Wessel and Smith, 1995) software were used to process seismic data.

References

Anguita, F., Hernán, F., 2000. The Canary Islands origin : a unifying model. J. Volcanol. Geotherm. Res. 103, 1–26. doi:10.1016/S0377-0273(00)00195-5

Arroucau, P., Custódio, S., Civiero, C., Dias, N. A., Silveira, G, 2017. PRISM3D: a preliminary 3D reference seismic model of the crust and upper mantle beneath Iberia. Geophys. Res. Abstracts, 19, EGU2017-16801, 2017

Ayarza, P., Carbonell, R., Teixell, A., Palomeras, I., Marti, D., Kchikach, A., Harnafi, M., Levander, A., Gallart, J., Arboleya, M.L., Alcalde, J., Fernandez, M., Charroud, M., Amrhar, M., 2014. Crustal thickness and velocity structure across the Moroccan Atlas from long offset wide-angle reflection seismic data: The SIMA experiment. Geochemistry, Geophys. Geosystems 15, 1698–1717. doi:10.1002/2013GC005164

Ballmer, M.D., Conrad, C.P., Smith, E.I., Johnsen, R., 2015. Intraplate volcanism at the edges of the Colorado Plateau sustained by a combination of triggered edge-driven convection and shear-driven upwelling. Geochemistry, Geophys. Geosystems 16, 366–379. doi:10.1002/2014GC005641

Bastow, I.D., 2012. Relative arrival-time upper-mantle tomography and the elusive background mean. Geophys. J. Int. 190, 1271–1278. doi:10.1111/j.1365-246X.2012.05559.x

Bell, K., Castorina, F., Lavecchia, G., Rosatelli, G., Stoppa, F., 2004. Is there a mantle plume below Italy? Eos, Trans. Am. Geophys. Union 85, 541. doi:10.1029/2004EO500002

Bezada, M.J., Faccenda, M., Toomey, D.R., 2016. Representing anisotropic subduction zones with isotropic velocitymodels: A characterization of the problem and some steps on a possible path forward. Geochemistry Geophys. Geosystems 17, 2825–2834. doi:10.1002/2016GC006406

Bezada, M.J., Humphreys, E.D., Davila, J.M., Carbonell, R., Harnafi, M., Palomeras, I., Levander, A., 2014. Piecewise delamination of Moroccan lithosphere from beneath the Atlas Mountains. Geochemistry, Geophys. Geosystems 15, 975–985.

doi:10.1002/2013GC005059

Bezada, M.J., Humphreys, E.D., Toomey, D.R., Harnafi, M., Dávila, J.M., Gallart, J., 2013. Evidence for slab rollback in westernmost Mediterranean from improved upper mantle imaging. Earth Planet. Sci. Lett. 368, 51–60. doi:10.1016/j.epsl.2013.02.024

Bijwaard, H., Spakman, W., Engdahl, E.R., 1998. Closing the gap between regional and global travel time tomography. J. Geophys. Res. Solid Earth 103, 30055–30078. doi:10.1029/98JB02467

Bird, P., 2003. An updated digital model of plate boundaries. Geochemistry, Geophys. Geosystems 4. doi:10.1029/2001GC000252

Blanco, M.J., Spakman, W., 1993. The P-wave velocity structure of the mantle below the Iberian Peninsula : evidence for subducted lithosphere below southern Spain. Tectonophysics 221, 13–34. doi:https://doi.org/10.1016/0040-1951(93)90025-F

Bonatto, L., Schimmel, M., Gallart, J., Morales, J., 2015. The upper-mantle transition zone beneath the Ibero-Maghrebian region as seen by teleseismic Pds phases. Tectonophysics 663, 212–224. doi:10.1016/j.tecto.2015.02.002

Bonnin, M., Nolet, G., Villaseñor, A., Gallart, J., Thomas, C., 2014. Multiple-frequency tomography of the upper mantle beneath the African/Iberian collision zone. Geophys. J. Int. 198, 1458–1473. doi:10.1093/gji/ggu214

Boschi, L., Becker, T.W., Steinberger, B., 2007. Mantle plumes: Dynamic models and seismic images. Geochemistry, Geophys. Geosystems 8, 1–20. doi:10.1029/2007GC001733

Boschi, L., Ekström, G., Kustowski, B., 2004. Multiple resolution surface wave tomography: The Mediterranean basin. Geophys. J. Int. 157, 293–304. doi:10.1111/j.1365-246X.2004.02194.x

Bossmann, A.B., Van Keken, P.E., 2013. Dynamics of plumes in a compressible mantle with phase changes: Implications for phase boundary topography. Phys. Earth Planet. Inter. 224, 21–31. doi:10.1016/j.pepi.2013.09.002

Buontempo, L., Bokelmann, G.H.R., Barruol, G., Morales, J., 2008. Seismic anisotropy beneath southern Iberia from SKS splitting. Earth Planet. Sci. Lett. 273, 237–250. doi:10.1016/j.epsl.2008.06.024

Cadoux, A., Blichert-Toft, J., Pinti, D.L., Albarède, F., 2007. A unique lower mantle source for Southern Italy volcanics. Earth Planet. Sci. Lett. 259, 227–238. doi:10.1016/j.epsl.2007.04.001

Carrara, G., and NEAREST Team, 2008. NEAREST 2008 CRUISE PRELIMINARY REPORT R/V URANIA, 1st Aug 2008- 04th Sept 2008, Technical Report ISMAR

Chang, S.J., Van Der Lee, S., Flanagan, M.P., Bedle, H., Marone, F., Matzel, E.M., Pasyanos, M.E., Rodgers, A.J., Romanowicz, B., Schmid, C., 2010. Joint inversion for three-dimensional S velocity mantle structure along the Tethyan margin. J. Geophys. Res. Solid Earth 115, 1–22. doi:10.1029/2009JB007204

Chevrot, S., Villasenor, A., Sylvander, M., Benahmed, S., Beucler, E., Cougoulat, G., Delmas, P., Blanquat, M.D. Saint, Diaz, J., Gallart, J., Grimaud, F., Lagabrielle, Y., Manatschal, G., Mocquet, A., Pauchet, H., Paul, A., Péquegnat, C., Quillard, O., Roussel, S., Ruiz, M., Wolyniec, D., 2014. High-resolution imaging of the Pyrenees and Massif Central from the data of the PYROPE and IBERARRAY portable array deployments. J. Geophys. Res. B Solid Earth 119, 6399–6420. doi:10.1002/2014JB010953

Civiero, C., Goes, S., Hammond, J.O.S., Fishwick, S., Ahmed, A., Ayele, A., Doubre, C., Goitom, B., Keir, D., Kendall, J.M., Leroy, S., Ogubazghi, G., Rümpker, G., Stuart, G.W., 2016. Small-scale thermal upwellings under the northern East African Rift from S travel time tomography. J. Geophys. Res. Solid Earth 2010, 1–14. doi:10.1002/2016JB013070

Civiero, C., Hammond, J.O.S., Goes, S., Fishwick, S., Ahmed, A., Ayele, A., Doubre, C., Goitom, B., Keir, D., Kendall, J.M., Leroy, S., Ogubazghi, G., Rümpker, G., Stuart, G.W., 2015. Multiple mantle upwellings in the transition zone beneath the northern East-African Rift system from relative P-wave travel-time tomography. Geochemistry, Geophys. Geosystems 16, 2949–2968. doi:10.1002/2015GC005948

Cserepes, L., Yuen, D.A., 2000. On the possibility of a second kind of mantle plume. Earth Planet. Sci. Lett. 183, 61–71. doi:10.1016/S0012-821X(00)00265-X

Custódio, S., Dias, N.A., Caldeira, B., Carrilho, F., Carvalho, S., Corela, C., Díaz, J., Narciso, J., Madureira, G., Matias, L., Haberland, C., 2014. Ambient noise recorded by a dense broadband seismic deployment in Western Iberia. Bull. Seismol. Soc. Am. 104, 2985–3007. doi:10.1785/0120140079

Davaille, A., Stutzmann, E., Silveira, G., Besse, J., Courtillot, V., 2005. Convective patterns under the Indo-Atlantic « box ». Earth Planet. Sci. Lett. 239, 233–252. doi:10.1016/j.epsl.2005.07.024

de Kool, M., Rawlinson, N., Sambridge, M., 2006. A practical grid-based method for tracking multiple refraction and reflection phases in three-dimensional heterogeneous media. Geophys. J. Int. 167, 253–270. doi:10.1111/j.1365-246X.2006.03078.x

Deuss, A., 2007. Seismic observations of transition-zone discontinuities beneath hotspot locations. Spec. Pap. 430 Plates, Plumes Planet. Process. 121–136. doi:10.1130/2007.2430(07)

Díaz, J., Gallart, J., Morais, I., Silveira, G., Pedreira, D., Pulgar, J.A., Dias, N.A., Ruiz, M., González-cortina, J.M., 2015. Tectonophysics From the Bay of Biscay to the High Atlas : Completing the anisotropic characterization of the upper mantle beneath the westernmost Mediterranean region. Tectonophysics. doi:10.1016/j.tecto.2015.03.007

Díaz, J., Gallart, J., Villaseñor, A., Mancilla, F., Pazos, A., Córdoba, D., Pulgar, J.A., Ibarra, P., Harnafi, M., 2010. Mantle dynamics beneath the Gibraltar Are (western Mediterranean) from shear-wave splitting measurements on a dense seismic array. Geophys. Res. Lett. 37, 1–5. doi:10.1029/2010GL044201

Druken, K.A., Kincaid, C., Griffiths, R.W., Stegman, D.R., Hart, S.R., 2014. Plume-slab interaction: The Samoa-Tonga system. Phys. Earth Planet. Inter. 232, 1–14. doi:10.1016/j.pepi.2014.03.003

Duggen, S., Hoernle, K.A., Hauff, F., Klügel, A., Bouabdellah, M., Thirlwall, M.F., 2009. Flow of Canary mantle plume material through a subcontinental lithospheric corridor beneath Africa to the Mediterranean. Geology 37, 283–286. doi:10.1130/G25426A.1

Duggen, S., Hoernle, K., van den Bogaard, P., Garbe-Schönberg, D., 2005. Post-collisional transition from subduction-to intraplate-type magmatism in the westernmost Mediterranean: Evidence for continental-edge delamination of subcontinental lithosphere. J. Petrol. 46, 1155–1201. doi:10.1093/petrology/egi013

Duggen, S., Hoernle, K., van den Bogaard, P., Harris, C., 2004. Magmatic evolution of the Alboran region: The role of subduction in forming the western Mediterranean and causing the Messinian Salinity Crisis. Earth Planet. Sci. Lett. 218, 91–108. doi:10.1016/S0012-821X(03)00632-0

El Azzouzi, E., El, M., Mohammed, A., Universit, M., Occidentale, B., Universit, B., Occidentale, B., 2010. Petrology and K-Ar chronology of the Neogene- Quaternary Middle Atlas basaltic province , Morocco. Bull. la Société Géologique Fr. doi:10.2113/gssgfbull.181.3.243

Fernandes, R.M.S., Ambrosius, B.A.C., Noomen, R., Bastos, L., Wortel, M.J.R., Spakman, W., Govers, R., 2003. The relative motion between Africa and Eurasia as derived from ITRF2000 and GPS data. Geophys. Res. Lett. 30, 1–5. doi:10.1029/2003GL017089

Fichtner, A., Trampert, J., Cupillard, P., Saygin, E., Taymaz, T., Capdeville, Y., Villaseñor, A., 2013. Multiscale full waveform inversion. Geophys. J. Int. 194, 534–556. doi:10.1093/gji/ggt118

French, S.W., Romanowicz, B., 2015. Broad plumes rooted at the base of the Earth's mantle beneath major hotspots. Nature 525, 95–99. doi:10.1038/nature14876

Frizon de Lamotte, D.F., Leturmy, P., Missenard, Y., Khomsi, S., Ruiz, G., Saddiqi, O., Guillocheau, F., Michard, A., 2009. Mesozoic and Cenozoic vertical movements in the Atlas system (Algeria, Morocco, Tunisia): An overview. Tectonophysics 475, 9–28. doi:10.1016/j.tecto.2008.10.024

Fullea, J., Fernàndez, M., Afonso, J.C., Vergés, J., Zeyen, H., 2010. The structure and evolution of the lithosphere-asthenosphere boundary beneath the Atlantic-Mediterranean Transition Region. Lithos 120, 74–95. doi:10.1016/j.lithos.2010.03.003

Funiciello, F., Moroni, M., Piromallo, C., Faccenna, C., Cenedese, A., Bui, H.A., 2006. Mapping mantle flow during retreating subduction: Laboratory models analyzed by feature tracking. J. Geophys. Res. Solid Earth 111, 1–16. doi:10.1029/2005JB003792

Gasperini, D., Blichert-Toft, J., Bosch, D., Del Moro, A., Macera, P., Albarède, F., 2002. Upwelling of deep mantle material through a plate window: Evidence from the geochemistry of Italian basaltic volcanics. J. Geophys. Res. Solid Earth 107, ECV 7-1-ECV 7-19. doi:10.1029/2001JB000418

Granet, M., Wilson, M., Achauer, U., 1995. Imaging a mantle plume beneath the French Massif Central. Earth Planet. Sci. Lett. 136, 281–296. doi:10.1016/0012-821X(95)00174-B

Grevemeyer, I. e. a. FS Poseidon POS389 & POS393 & FS Maria S. Merian MSM15/5: TOPOMED- Topographic, structural and seismotectonic consequences of plate re-organization in the Gulf of Cadiz and Alboran Sea, POS389: Valletta, Malta – Malaga, Spain, 06.–17.08.2009; POS393: Malaga, Spain – Faro, Portugal, 14.–24.01.2010, MSM15/5: Valletta, Malta - Rostock, Germany, 17.–29.07.2010. IFM-GEOMAR Report, 45. IFM-GEOMAR, Kiel, page 41 pp, 2011. doi:10.3289/ifmgeomar_rep_45_2011

Gutscher, M.A., Malod, J., Rehault, J.P., Contrucci, I., Klingelhoefer, F., Mendes-Victor, L., Spakman, W., 2002. Evidence for active subduction beneath Gibraltar. Geology 30, 1071–1074. doi:10.1130/0091-7613(2002)030<1071:EFASBG>2.0.CO;2

Helffrich, G., Wookey, J., Bastow I., (2013), The Seismic Analysis Code: A Primer and User's Guide, Cambridge Univ. Press, Cambridge, U. K.

Hoernle, K., van den Bogaard, P., Duggen, S., Mocek, B., Garbe-Schönberg, D., 1999. Evidence for Miocene subduction beneath the Alboran Sea: 40Ar/39Ar dating and geochemistry of volcanic rocks from Holes 977A and 978A. Proc. Ocean Drill. Progr. 161, 357–373. doi:10.2973/odp.proc.sr.161.264.1999

Hoernle, K., Zhang, Y.-S., Graham, D., 1995. Seismic and geochemical evidence for large-scale mantle upwelling beneath the eastern Atlantic and western and central Europe. Nature. 374, 34–39. doi:10.1038/374034a0

Houser, C., Masters, G., Flanagan, M., Shearer, P., 2008. Determination and analysis of long-wavelength transition zone structure using SS precursors. Geophys. J. Int. 174, 178–194. doi:10.1111/j.1365-246X.2008.03719.x

International Seismological Centre, *On-line Bulletin*, http://www.isc.ac.uk, Internatl. Seismol. Cent., Thatcham, United Kingdom, 2015

Kaislaniemi, Van Hunen, J., 2014. Dynamics of lithospheric thinning and mantle melting by edge-driven convection: Application to Moroccan Atlas mountains. Geochemistry, Geophys. Geosystems 158, 3175–3189. doi:10.1002/2015GC005918

Kárason, H., van der Hilst, R.D., 2001. Tomographic imaging of the lowermost mantle with differential times of refracted and diffracted core phases (PKP, Pdiff). J. Geophys. Res. Solid Earth 106, 6569–6587. doi:10.1029/2000JB900380

Kennett, B.L.N., Engdahl, E.R., Buland, R., 1995. Constraints on seismic velocities in the Earth from travel times. Geophys. J. Int. 122, 108–124. doi:10.1111/j.1365-246X.1995.tb03540.x

Kennett, B.L.N., Sambridge, M., Williamson, P.R., 1988. Subspace methods for large inverse problems with multiple parameter classes. Geophys. J. Int. 94, 237–247. doi:10.1111/j.1365-246X.1988.tb05898.x

Kincaid, C., Druken, K.A., Griffiths, R.W., Stegman, D.R., 2013. Bifurcation of the Yellowstone plume driven by subduction-induced mantle flow. Nat. Geosci. 6, 395–399. doi:10.1038/ngeo1774

Koulakov, I., Kaban, M.K., Tesauro, M., Cloetingh, S., 2009. P- and S-velocity anomalies in the upper mantle beneath Europe from tomographic inversion of ISC data. Geophys. J. Int. 179, 345–366. doi:10.1111/j.1365-246X.2009.04279.x

Kumagai, I., Davaille, A., Kurita, K., 2007. On the fate of thermally buoyant mantle plumes at density interfaces. Earth Planet. Sci. Lett. 254, 180–193.

doi:10.1016/j.epsl.2006.11.029

Lawrence, J.F., Shearer, P.M., 2006. A global study of transition zone thickness using receiver functions. J. Geophys. Res. Solid Earth 111, 1–10. doi:10.1029/2005JB003973

Leng, W., Gurnis, M., 2012. Shape of thermal plumes in a compressible mantle with depth-dependent viscosity. Geophys. Res. Lett. 39, 1–7. doi:10.1029/2012GL050959

Levander, A., Bezada, M.J., Niu, F., Humphreys, E.D., Palomeras, I., Thurner, S.M., Masy, J., Schmitz, M., Gallart, J., Carbonell, R., Miller, M.S., 2014. Subduction-driven recycling of continental margin lithosphere. Nature 515, 253–256. doi:10.1038/nature13878

Li, C., Van Der Hilst, R.D., Engdahl, E.R., Burdick, S., 2008. A new global model for P wave speed variations in Earth's mantle. Geochemistry, Geophys. Geosystems 9, Q05018. doi:10.1029/2007GC001806

Li, Z.H., Ribe, N.M., 2012. Dynamics of free subduction from 3-D boundary element modeling. J. Geophys. Res. Solid Earth 117, 1–18. doi:10.1029/2012JB009165

Lodge, A., Nippress, S.E.J., Rietbrock, A., García-Yeguas, A., Ibáñez, J.M., 2012. Evidence for magmatic underplating and partial melt beneath the Canary Islands derived using teleseismic receiver functions. Phys. Earth Planet. Inter. 212–213, 44–54. doi:10.1016/j.pepi.2012.09.004

Lustrino, M., Wilson, M., 2007. The circum-Mediterranean anorogenic Cenozoic igneous province. Earth-Science Rev. 81, 1–65. doi:doi:10.1016/j.earscirev.2006.09.002

Martinez-Arevalo, C., Mancilla, F. de L., Helffrich, G., Garcia, A., 2013. Seismic evidence of a regional sublithospheric low velocity layer beneath the Canary Islands. Tectonophysics 608, 586–599. doi:10.1016/j.tecto.2013.08.021

Mauffret, A., 2007. The Northwestern (Maghreb) boundary of the Nubia (Africa) Plate. Tectonophysics 429, 21–44. doi:10.1016/j.tecto.2006.09.007

Maury, R., Fourcade, S., Coulon, C., El Azzouzi, M., Bellon, H., Coutelle, A., Ouabadi, A., Semroud, B., Megartsi, M., Cotten, J., Belanteur, O., Louni-Hacini, A., Piqué, A., Capdevila, R., Hernandez, J., Réhault, J.P., 2000. Post-collisional Neogene magmatism of the Mediterranean Maghreb margin: A consequence of slab breakoff. Comptes Rendus l'Academie Sci. - Ser. IIa Sci. la Terre des Planetes 331, 159–173. doi:10.1016/S1251-8050(00)01406-3

Mériaux, C.A., Duarte, J.C., Duarte, S.S., Schellart, W.P., Chen, Z., Rosas, F., Mata, J., Terrinha, P., 2015a. Capture of the Canary mantle plume material by the Gibraltar arc mantle wedge during slab rollback. Geophys. J. Int. 201, 1717–1721. doi:10.1093/gji/ggv120

Mériaux, C.A., Duarte, J.C., Schellart, W.P., Mériaux, A.S., 2015b. A two-way interaction between the Hainan plume and the Manila subduction zone. Geophys. Res. Lett. 42, 5796–5802. doi:10.1002/2015GL064313

Mériaux, C.A., Mériaux, A.-S., Schellart, W.P., Duarte, J.C., Duarte, S.S., Chen, Z., 2016. Mantle plumes in the vicinity of subduction zones. Earth Planet. Sci. Lett. 454, 166–177. doi:10.1016/j.epsl.2016.09.001

Miller, M.S., Allam, A.A., Becker, T.W., Di Leo, J.F., Wookey, J., 2013. Constraints on the tectonic evolution of the westernmost Mediterranean and northwestern Africa from shear wave splitting analysis. Earth Planet. Sci. Lett. 375, 234–243. doi:10.1016/j.epsl.2013.05.036

Miller, M.S., Becker, T.W., 2014. Reactivated lithospheric-scale discontinuities localize dynamic uplift of the Moroccan Atlas Mountains. Geology 42, 35–38. doi:10.1130/G34959.1

Miller, M.S., Driscoll, L.J.O., Butcher, A.J., Thomas, C., 2015. Imaging Canary Island hotspot material beneath the lithosphere of Morocco and southern Spain. Earth Planet. Sci. Lett. 431, 186–194. doi:10.1016/j.epsl.2015.09.026

Missenard, Y., Cadoux, A., 2012. Can Moroccan Atlas lithospheric thinning and volcanism be induced by Edge-Driven Convection ? Terra Nov. 24, 27–33. doi:10.1111/j.1365-3121.2011.01033.x

Missenard, Y., Zeyen, H., de Lamotte, D.F., Leturmy, P., Petit, C., Sébrier, M., Saddiqi, O., 2006. Crustal versus asthenospheric origin of relief of the Atlas mountains of Morocco.

J. Geophys. Res. Solid Earth 111, 1–13. doi:10.1029/2005JB003708

Monna, S., Cimini, G.B., Montuori, C., Matias, L., Geissler, W.H., Favali, P., 2013. New insights from seismic tomography on the complex geodynamic evolution of two adjacent domains: Gulf of Cadiz and Alboran Sea. J. Geophys. Res. Solid Earth 118, 1587–1601. doi:10.1029/2012JB009607

Montelli, R., Nolet, G., Dahlen, F.., Masters, G., Engdahl, E.R., Hung, S.H., 2004. Finite-Frequency Tomography Reveals a Variety of Plumes in the Mantle. Science (80-.). 303, 338–343. doi:10.1126/science.1092485

Montelli, R., Nolet, G., Dahlen, F.A., Masters, G., 2006. A catalogue of deep mantle plumes: New results from finitefrequency tomography. Geochemistry, Geophys. Geosystems 7, (11). doi:10.1029/2006GC001248

Morgan, W.J., 1972. Deep Mantle Convection Plumes and Plate Motions. Am. Assoc. Pet. Geol. Bull. doi:10.1306/819A3E50-16C5-11D7-8645000102C1865D

Neres, M., Carafa, M.M.C., Fernandes, R.M.S., Matias, L., Duarte, J.C., Barba, S., Terrinha, P., 2016. Lithospheric deformation in the Africa-Iberia plate boundary: Improved neotectonic modeling testing a basal-driven Alboran plate. J. Geophys. Res. Solid Earth 121, 6566–6596. doi:10.1002/2016JB013012

Oyarzun, R., Doblas, M., López-Ruiz, J., Cebrá, J.M., 1997. Opening of the central Atlantic and asymmetric mantle upwelling phenomena : Implications for long-lived magmatism in western North Africa and Europe Geology, 727–730.

Palomeras, I., Villaseñor, A., Thurner, S., Levander, A., Gallart, J., Harnafi, M., 2017. Lithospheric structure of Iberia and Morocco using finite-frequency Rayleigh wave tomography from earthquakes and seismic ambient noise. Geochemistry, Geophys. Geosystems 1824–1840. doi:10.1002/2016GC006657

Palomeras, I., Thurner, S., Levander, A., Liu, K., Villasenor, A., Carbonell, R., Harnafi, M., 2014. Finite-frequency Rayleigh wave tomography of the western Mediterranean: Mapping its lithospheric structure. Geochemistry, Geophys. Geosystems 15, 140–160. doi:10.1002/2013GC004861

Pérez-Valera, L.A., Rosenbaum, G., Sánchez-Gómez, M., Azor, A., Fernández-Soler, J.M., Pérez-Valera, F., Vasconcelos, P.M., 2013. Age distribution of lamproites along the Socovos Fault (southern Spain) and lithospheric scale tearing. Lithos 180–181, 252–263. doi:10.1016/j.lithos.2013.08.016

Piromallo, C., Becker, T.W., Funiciello, F., Faccenna, C., 2006. Three-dimensional instantaneous mantle flow induced by subduction. Geophys. Res. Lett. 33, 5–8. doi:10.1029/2005GL025390

Piromallo, C., Gasperini, D., Macera, P., Faccenna, C., 2008. A late Cretaceous contamination episode of the European – Mediterranean mantle. Earth Planet. Sci. Lett. 268, 15–27. doi:10.1016/j.epsl.2007.12.019

Piromallo, C., Morelli, A., 2003. *P* wave tomography of the mantle under the Alpine-Mediterranean area. J. Geophys. Res. Solid Earth 108, 1–23. doi:10.1029/2002JB001757

Platt, J.P., Becker, T. W., Evans, TR.L., Humphreys, E.D., Lee, C.-T., Levander A., 2008. PICASSO: Testing Models for Upper Mantle Processes Beneath the Alboran Basin and the Gibraltar Arc (Western Mediterranean). Paper presented at AGU General Assembly, American Geosciences Union, San Francisco, USA (2008)

Ramdani, F., 1998. Geodynamic implications of intermediate-depth earthquakes and volcanism in the intraplate Atlas Mountains (Morocco). Phys. Earth Planet. Inter. 108, 245–260. doi:10.1016/S0031-9201(98)00106-X

Rawlinson, N., Fishwick, S., 2012. Seismic structure of the southeast Australian lithosphere from surface and body wave tomography. Tectonophysics 572–573, 111–122. doi:10.1016/j.tecto.2011.11.016

Rawlinson, N., Kennett, B.L.N., 2004. Rapid estimation of relative and absolute delay times across a network by adaptive stacking. Geophys. J. Int. 157, 332–340. doi:10.1111/j.1365-246X.2004.02188.x

Rawlinson, N., Pozgay, S., Fishwick, S., 2010. Seismic tomography: A window into deep Earth. Phys. Earth Planet. Inter. 178, 101–135. doi:10.1016/j.pepi.2009.10.002

Rawlinson, N., Reading, A.M., Kennett, B.L.N., 2006. Lithospheric structure of Tasmania from a novel form of teleseismic tomography. J. Geophys. Res. Solid Earth 111, 1–21. doi:10.1029/2005JB003803

Rawlinson, N., Salmon, M., Kennett, B.L.N., 2014. Transportable seismic array tomography in southeast Australia: Illuminating the transition from Proterozoic to Phanerozoic lithosphere. Lithos 189, 65–76. doi:10.1016/j.lithos.2013.06.001

Rawlinson, N., Sambridge, M., 2004. Wave front evolution in strongly heterogeneous layered media using the fast marching method. Geophys. J. Int. 156, 631–647. doi:10.1111/j.1365-246X.2004.02153.x

Rawlinson, N., Urvoy, M., 2006. Simultaneous inversion of active and passive source datasets for 3-D seismic structure with application to Tasmania. Geophys. Res. Lett. 33, 1–5. doi:10.1029/2006GL028105

Ritsema, J., Deuss, A., Van Heijst, H.J., Woodhouse, J.H., 2011. S40RTS: A degree-40 shear-velocity model for the mantle from new Rayleigh wave dispersion, teleseismic traveltime and normal-mode splitting function measurements. Geophys. J. Int. 184, 1223–1236. doi:10.1111/j.1365-246X.2010.04884.x

Ritter, J.R.R., Jordan, M., Christensen, U.R., Achauer, U., 2001. A mantle plume below the Eifel volcanic fields, Germany. Earth Planet. Sci. Lett. 186, 7–14. doi:10.1016/S0012-821X(01)00226-6

Saki, M., Thomas, C., Nippress, S.E.J., Lessing, S., 2015. Topography of upper mantle seismic discontinuities beneath the North Atlantic : The Azores , Canary and Cape Verde plumes. Earth Planet. Sci. Lett. 409, 193–202. doi:10.1016/j.epsl.2014.10.052

Schaeffer, A.J., Lebedev, S., 2013. Global shear speed structure of the upper mantle and transition zone. Geophys. J. Int. 194, 417–449. doi:10.1093/gji/ggt095

Schellart, W.P., 2008. Kinematics and flow patterns in deep mantle and upper mantle subduction models: Influence of the mantle depth and slab to mantle viscosity ratio. Geochemistry, Geophys. Geosystems 9, Q03014. doi:10.1029/2007GC001656

Schivardi, R., Morelli, A., 2009. Surface wave tomography in the European and

Mediterranean region. Geophys. J. Int. 177, 1050–1066. doi:10.1111/j.1365-246X.2009.04100.x

Serpelloni, E., Vannucci, G., Pondrelli, S., Argnani, A., Casula, G., Anzidei, M., Baldi, P., Gasperini, P., 2007. Kinematics of the Western Africa-Eurasia plate boundary from focal mechanisms and GPS data. Geophys. J. Int. 169, 1180–1200. doi:10.1111/j.1365-246X.2007.03367.x

Sethian, J.A., 1996. A fast marching level set method for monotonically advancing fronts. Pnas 93, 1591–1595. doi:10.1073/pnas.93.4.1591

Simmons, N.A., Forte, A.M., Boschi, L., Grand, S.P., 2010. GyPSuM: A joint tomographic model of mantle density and seismic wave speeds. J. Geophys. Res. Solid Earth 115, 1–24. doi:10.1029/2010JB007631

Simmons, N.A., Myers, S.C., Johannesson, G., Matzel, E., 2012. LLNL-G3Dv3: Global P wave tomography model for improved regional and teleseismic travel time prediction. J. Geophys. Res. Solid Earth 117. doi:10.1029/2012JB009525

Smith, G.P., Wiens, D.A., Fischer, K.M., Dorman, L.M., Webb, S.C., Hildebrand, J.A., 2001. A Complex Pattern of Mantle Flow in the Lau Backarc. Science (80-.). 292, 713–716. doi:10.1126/science.1058763

Souriau, A., Chevrot, S., Olivera, C., 2008. A new tomographic image of the Pyrenean lithosphere from teleseismic data. Tectonophysics 460, 206–214. doi:10.1016/j.tecto.2008.08.014

Spakman, W., van der Lee, S., van der Hilst, R., 1993. Travel-time tomography of the European-Mediterranean mantle down to 1400 km. Phys. Earth Planet. Inter. 79, 3–74. doi:10.1016/0031-9201(93)90142-V

Spieker, K., Wölbern, I., Thomas, C., Harnafi, M., Moudnib, L. El, 2014. Crustal and upper-mantle structure beneath the western Atlas Mountains in SW Morocco derived from receiver functions. Geophys. J. Int. 198, 1474–1485. doi:10.1093/gji/ggu216

Stegman, D.R., Freeman, J., Schellart, W.P., Moresi, L., May, D., 2006. Influence of trench width on subduction hinge retreat rates in 3-D models of slab rollback. Geochemistry,

Geophys. Geosystems 7, Q03012. doi:10.1029/2005GC001056
Stich, D., Serpelloni, E., Lis, F. De, Morales, J., 2006. Kinematics of the Iberia – Maghreb plate contact from seismic moment tensors and GPS observations. Tectonophysics 426, 295–317. doi:10.1016/j.tecto.2006.08.004
Strak, V., Schellart, W.P., 2014. Evolution of 3-D subduction-induced mantle flow around lateral slab edges in analogue models of free subduction analysed by stereoscopic particle image velocimetry technique. Earth Planet. Sci. Lett. 403, 368–379. doi:10.1016/j.epsl.2014.07.007
Sun, D., Miller, M.S., Holt, A.F., Becker, T.W., 2014. Hot upwelling conduit beneath the Atlas Mountains, Morocco. Geophys. Res. Lett. 391, 212–223. doi:10.1002/2014GL061884
Teixell, A., Ayarza, P., Zeyen, H., Fernàndez, M., Arboleya, M.L., 2005. Effects of mantle upwelling in a compressional setting: The Atlas Mountains of Morocco. Terra Nov. 17, 456–461. doi:10.1111/j.1365-3121.2005.00633.x
Tesoniero, A., Auer, L., Boschi, L., Cammarano, F., 2015. Hydration of marginal basins and compositional variations within the continental lithospheric mantle inferred from a new global model of shear and compressional velocity. J. Geophys. Res. B Solid Earth 120, 7789–7813. doi:10.1002/2015JB012026
Thurner, S., Palomeras, I., Levander, A., Carbonell, R., Lee, C.T., 2014. Ongoing lithospheric removal in the western Mediterranean: Evidence from Ps receiver functions and thermobarometry of Neogene basalts (PICASSO project). Geochemistry, Geophys. Geosystems 15, 1113–1127. doi:10.1002/2013GC005124
Torres-Roldan, R.L., Poli, G., Peccerillo, A., 1986. An early Miocene arc-tholeitic magmatic dyke event from the Alboran sea: Evidence for precollision subduction and back-arc crustal extension in the westernmost Mediterranean. Geol. Rundschau 75, 219–234. doi:https://doi.org/10.1007/BF01770190
Tosi, N., Yuen, D.A., 2011. Bent-shaped plumes and horizontal channel flow beneath the 660km discontinuity. Earth Planet. Sci. Lett. 312, 348–359.

doi:10.1016/j.epsl.2011.10.015

Turner, S., Hawkesworth, C., 1998. Using geochemistry to map mantle flow beneath the Lau Basin. Geology 26, 1019–1022. doi:10.1130/0091-7613(1998)026<1019:UGTMMF>2.3.CO;2

Van Der Hilst, R.D., Widiyantoro, S., Engdahl, E.R., 1997. Evidence for deep mantle circulation from global tomography. Nature 386, 578-584. doi:10.1038/386578a0

van der Meijde, M., Marone, F., Giardini, D., Van Der Lee, S., 2003. Seismic Evidence for Water Deep in Earth's Upper Mantle. Science (80-.). 300, 1556–1558. doi:10.1126/science.1083636

van Keken, P.E., Gable, C.W., 1995. The Interaction of a Plume with a Rheological Boundary - a Comparison between 2-Dimensional and 3-Dimensional Models. J. Geophys. Res. Earth 100, 20291–20302. doi:0148-0227/95/95 JB-01152

Villaseñor, A., Chevrot, S., Harnafi, M., Gallart, J., Pazos, A., Serrano, I., Córdoba, D., Pulgar, J.A., Ibarra, P., 2015. Subduction and volcanism in the Iberia-North Africa collision zone from tomographic images of the upper mantle. Tectonophysics 663, 238–249. doi:10.1016/j.tecto.2015.08.042

Villaseñor, A., Ritzwoller, M.H., Levshin, A.L., Barmin, M.P., Engdahl, E.R., Spakman, W., Trampert, J., 2001. Shear velocity structure of central Eurasia from inversion of surface wave velocities. Phys. Earth Planet. Inter. 123, 169–184. doi:10.1016/S0031-9201(00)00208-9

Wessel, P., and Smith, W., 1995. New version of the Generic Mapping Tools released, Eos Trans. AGU, 76(33), 329, doi:10.1029/95EO00198

Wilson, M., Downes, H., 1991. Tertiary - Quarternary extension-related alkaline magmatism in Western and Central Europe. J. Petrol. 32, 811–849. doi:https://doi.org/10.1093/petrology/32.4.811

Wortel, M.J.R., Spakman, W., 2000. Subduction and Slab Detachment in the Mediterranean-Carpathian Region. Science (80-.). 290, 1910–1917. doi:10.1126/science.290.5498.1910

Zeyen, H., Ayarza, P., Fernàndez, M., Rimi, A., 2005. Lithospheric structure under the western African-European plate boundary: A transect across the Atlas Mountains and the Gulf of Cadiz. Tectonics 24, 1–16. doi:10.1029/2004TC001639

Zhao, D., 2007. Seismic images under 60 hotspots: Search for mantle plumes. Gondwana Res. 12, 335–355. doi:10.1016/j.gr.2007.03.001

Zhao, D., 2004. Global tomographic images of mantle plumes and subducting slabs: insight into deep Earth dynamics. Phys. Earth Planet. Int. 146, 3–34. doi:10.1016/j.pepi.2003.07.032

Zhu, H., Bozdăg, E., Tromp, J., 2015. Seismic structure of the European upper mantle based on adjoint tomography. Geophys. J. Int. 201, 18–52. doi:10.1093/gji/ggu492

Figure
Click here to download Figure: Figures_low_resolution.pdf

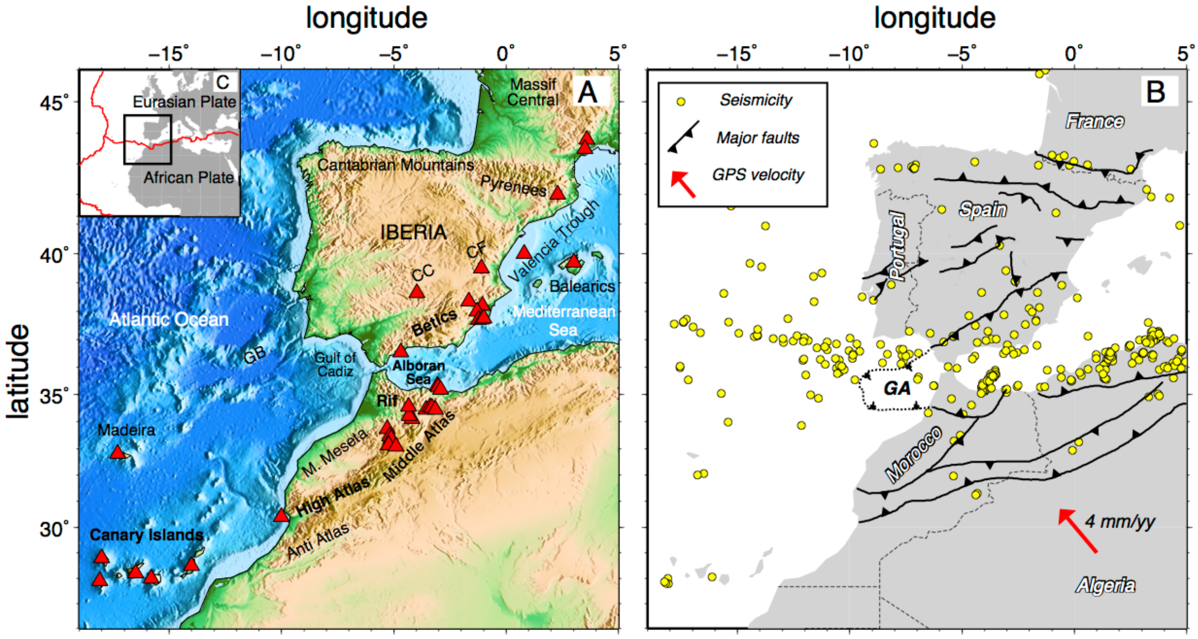

Figure 1. (A) Topography of the Ibero-western Maghreb region with the geographic features mentioned in the text marked up. *CC*: Calatrava volcanic province; *CF*: Cofrentes province; *GB*: Gorringe Bank. Cenozoic volcanic centres are represented with red triangles (modified from Lustrino and Wilson, 2007). (B) Simplified tectonic map of the Ibero-western Maghreb region. Relevant structural features (modified from Mauffret, 2007) are shown with black lines. The red arrow indicates the oblique GPS velocity (mm/yr) relative to the stable Iberia (Eurasia) reference frame (Fernandes et al., 2003; Serpelloni et al., 2007). Yellow circles represent seismicity (mb > 5.0) (International Seismological Centre, *On-line Bulletin*, http://www.isc.ac.uk, Internatl. Seismol. Cent., Thatcham, United Kingdom, 2015). *GA*: Gibraltar Arc. (C) Location of the Ibero-western Maghreb region along the Eurasia-Africa plate boundary. The red line shows the plate boundaries (from Bird, 2003).

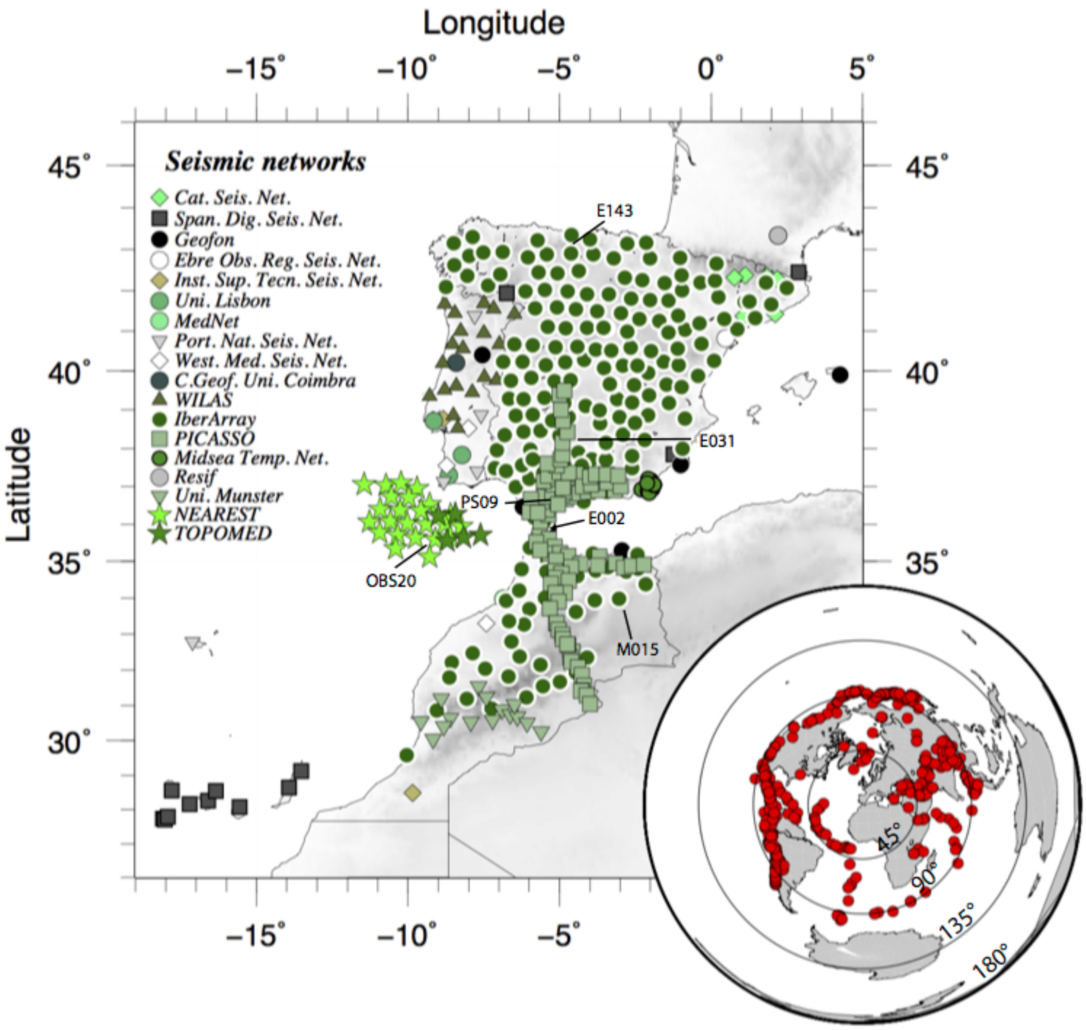

Figure 2. Distribution of seismic stations (green symbols in main map) and events (red dots in inset global map) used in this tomographic study. The stations are coded according to their network and cover an area extending from the Pyrenees in the north to Morocco and the Canaries in the south. The six labelled stations are those for which residuals are shown in Figure S4. Seismic experiment and station information can be found in Supplemental Information Tables ST1 and ST2.

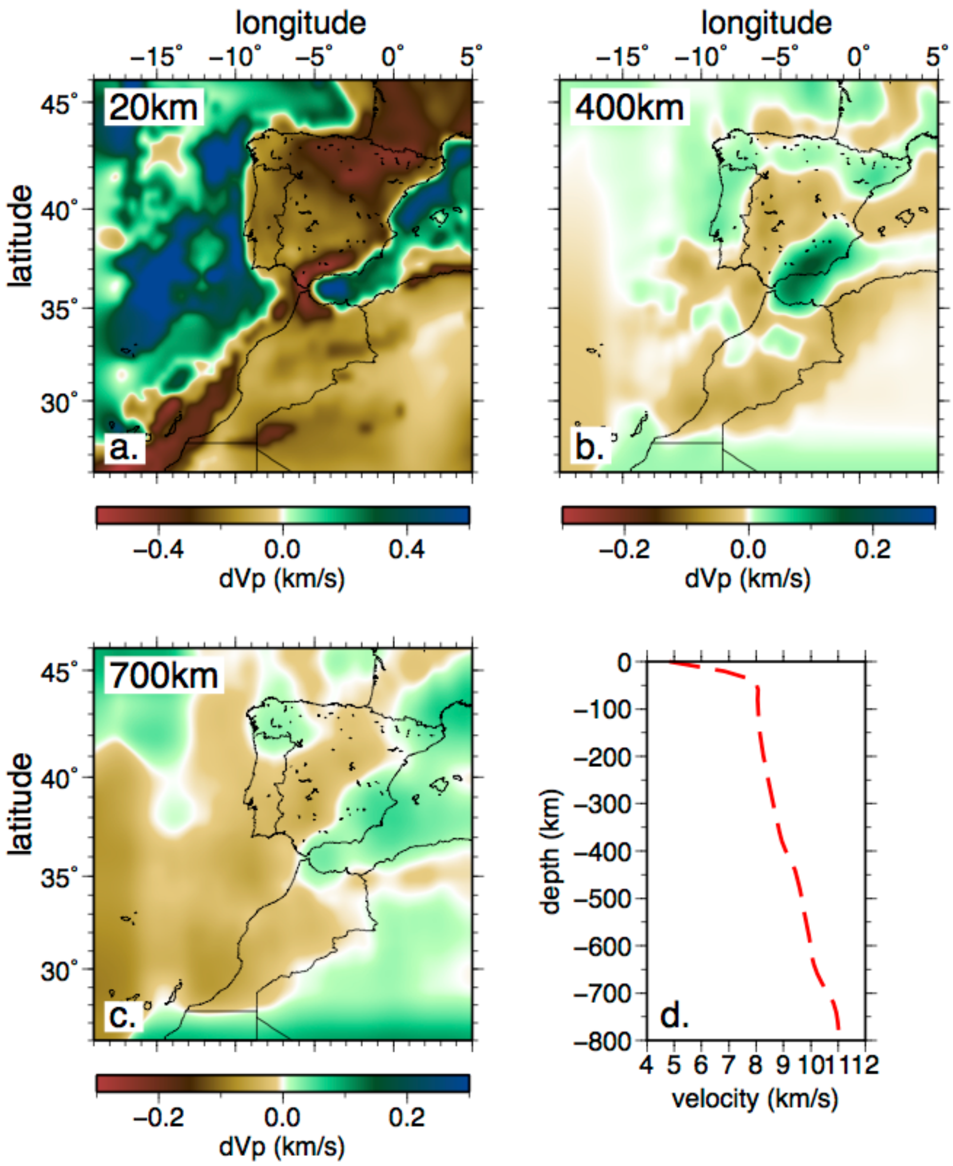

Figure 3. Depth slices through the starting model used for our tomographic inversion (*PRISM3D* down to 660 km depth and *LLNL* in 660-800 km depth range). (a) 20 km depth slice through the velocity model *PRISM3D*; (b) 400 km depth slice through the velocity model *PRISM3D*; (c) 700 km depth slice through the velocity model *LLNL*. (d) *1D* laterally averaged depth-dependent version of *PRISM3D* and *LLNL* model, used as a reference model for plotting the starting model and our final *P*-wave model.

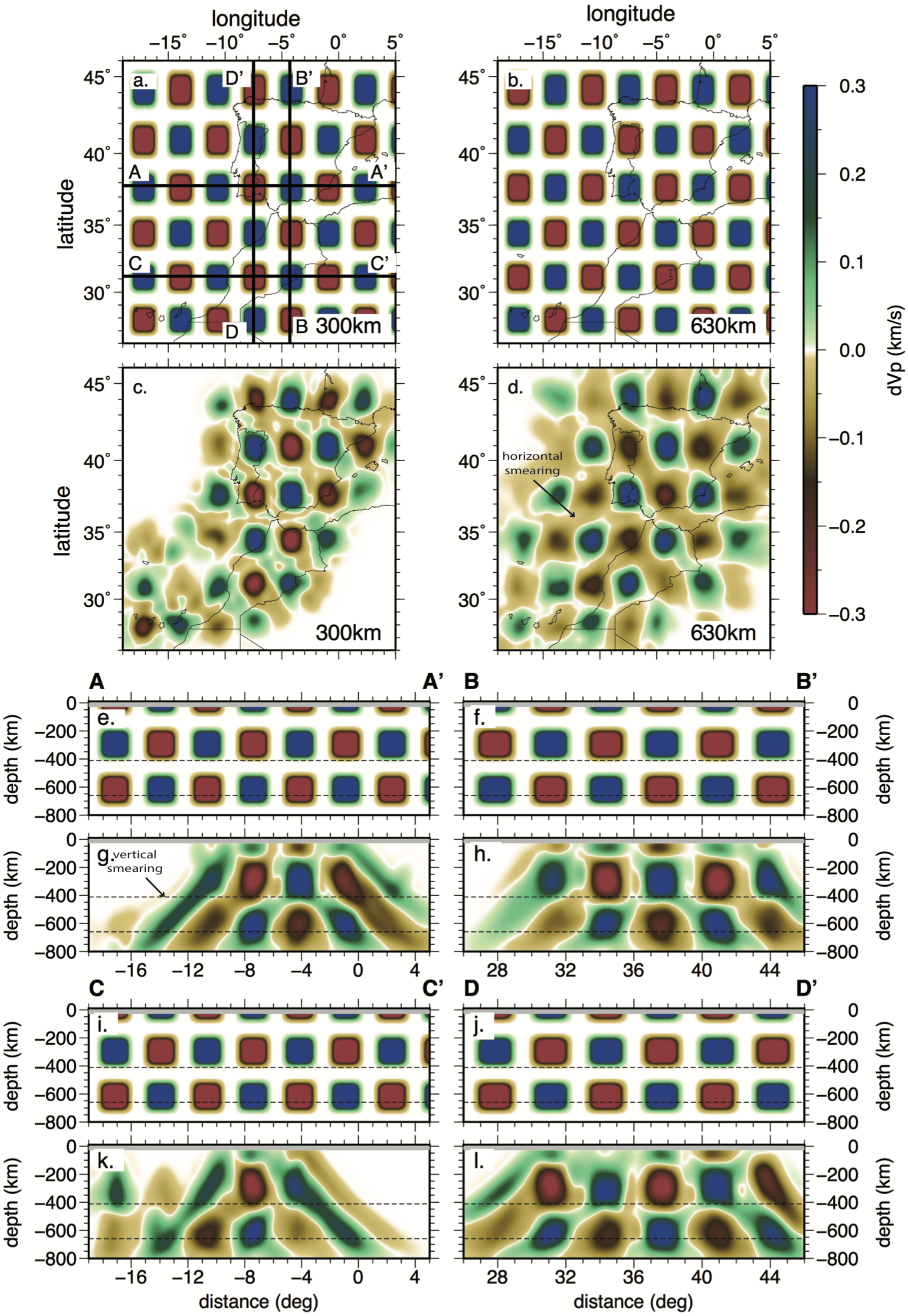

Figure 4. Checkerboard resolution tests for our tomographic study, using an alternating pattern of high- and low-velocity anomalies of ~140 km width and ±0.5 km/s in amplitude separated by a region of zero perturbation. In this case, velocity perturbations are plotted relative to the *3D* starting model. (a, b) Input model at 300 km and 630 km depth respectively. c, d) *P*-velocity structure at 300 km and 630 km depth respectively. The same raypaths and inversion parameters that are used in the inversion of the observations are used here. Gaussian noise of 0.1s standard deviation is added to the synthetic dataset to mimic the noise in the observations. Crustal structure is grey-shaded. These tests indicate a good resolution through the upper mantle for most of the region of interest, with the exception of the oceanic domain north of the Canaries and western African craton. (e, f, i, j) Vertical cross-sections

oriented east-west (e, i) and south-north (f, j), through the input model (orientations of the profiles are shown in depth slice a). (g, h, k, l) Vertical cross-sections through the recovered model. Resolution is good at least down to the base of the *MTZ* in Iberia and north-western Morocco, with smearing along rays at the edges of the region, especially beneath the oceanic domain.

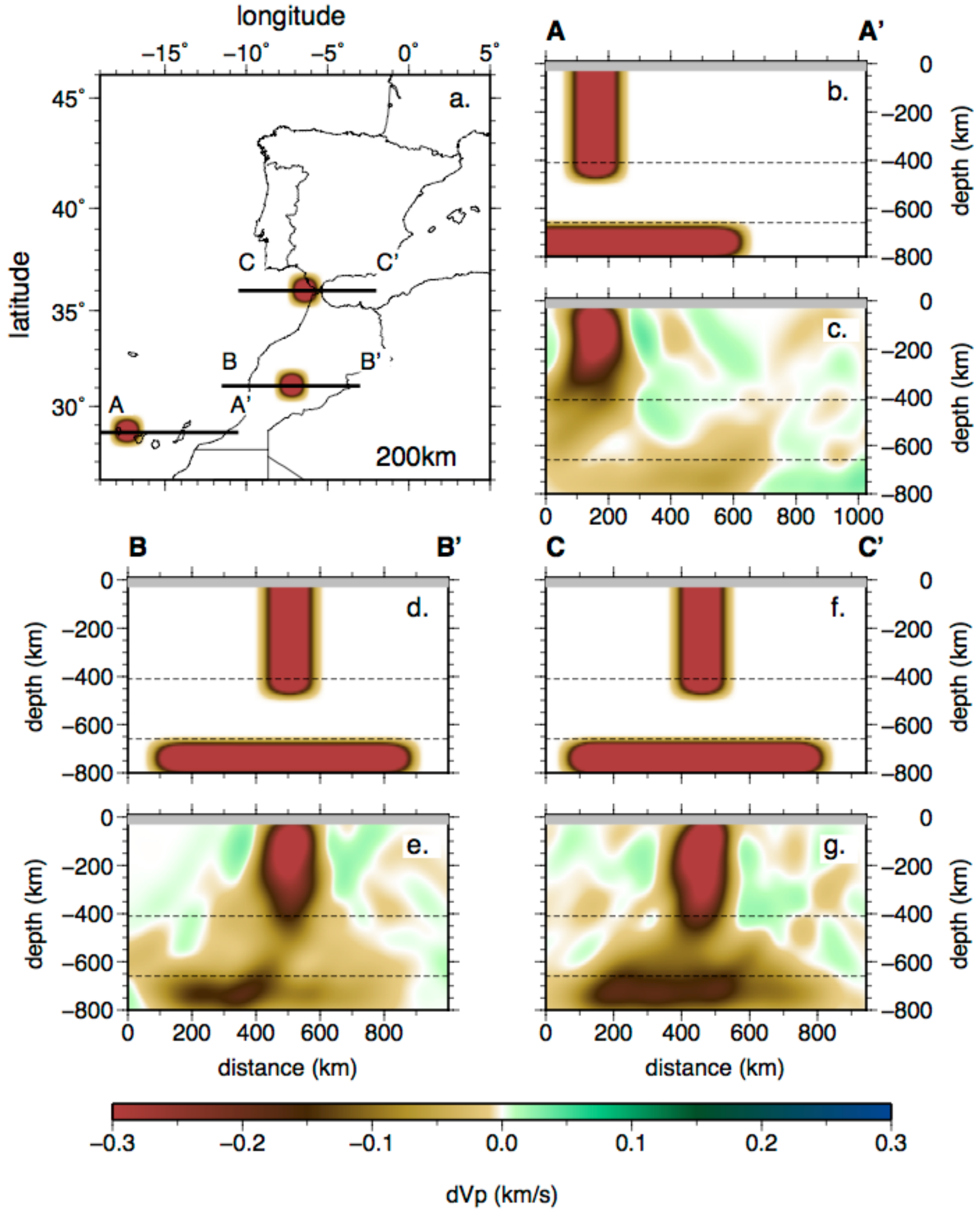

Figure 5. Structural resolution test for our tomographic study, using synthetic vertical low-velocity structures below the Canaries, the Atlas Ranges and the Gibraltar Arc and horizontal low-velocity layers below the *MTZ* (-0.5 km/s amplitude). Velocity perturbations are plotted relative to the *3D* starting model. (a) Map view of the input model at 200 km depth. (b, d, f) Input model through vertical cross-sections oriented west-east below the Canaries, the Atlas Ranges and the Gibraltar Arc respectively. Orientations of the profiles are shown in depth slice a). (c, e, g) Vertical cross-sections through the recovered model. The same raypaths and inversion parameters that are used in the inversion of the observations are used here and Gaussian noise of 0.1s standard deviation is added to the synthetic dataset to mimic the noise in the observations. Crustal structure is grey-shaded. Although an amount of smearing upward and downward is present, the vertical and horizontal bodies can be distinguished fairly well.

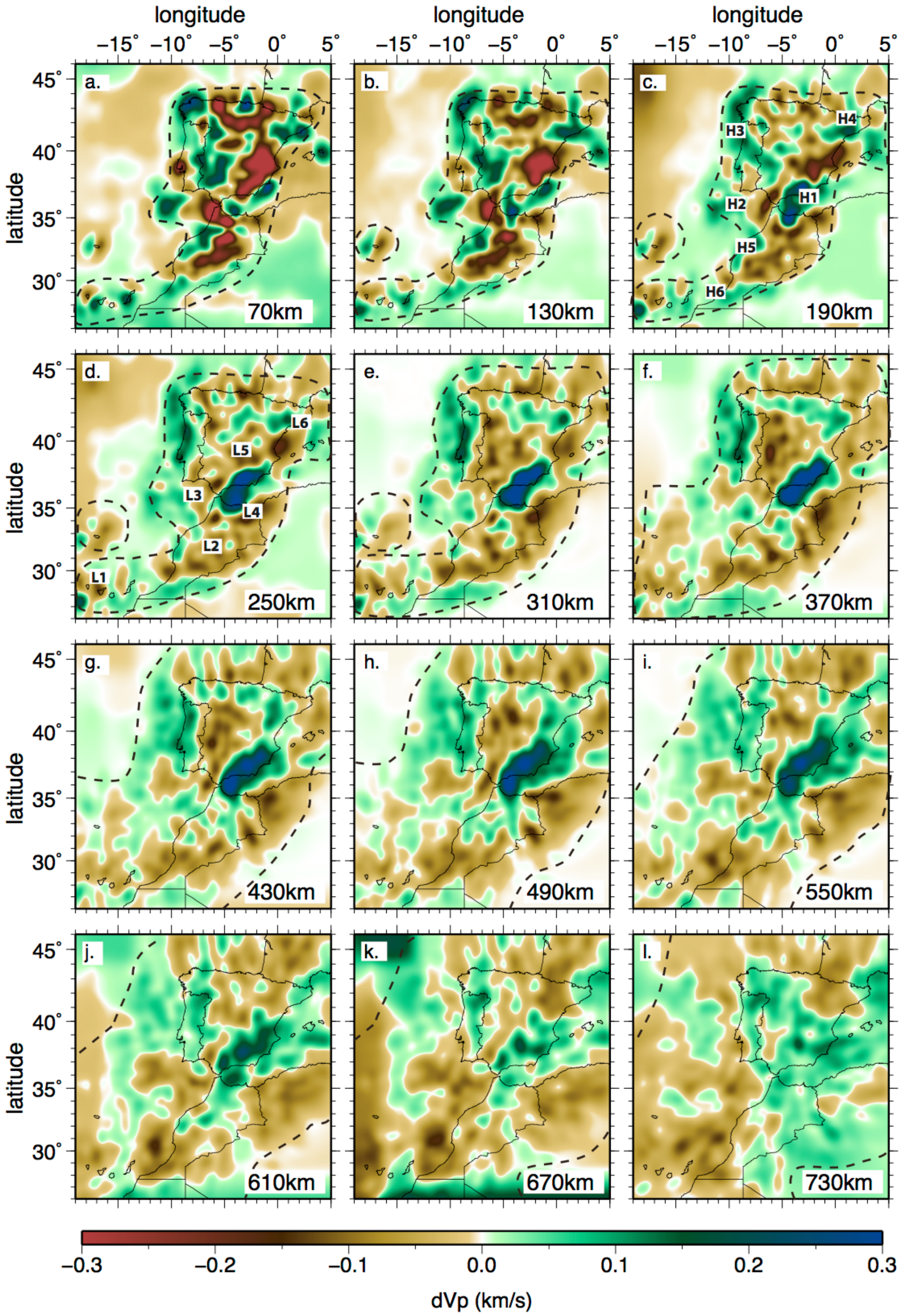

Figure 6. Depth slices through the tomographic *P*-wave model (damping = 5, smoothing = 5) at depths between 70 and 730 km. High-velocity anomalies mentioned in the text are identified in panel c and low-velocity anomalies are identified in panel d. Velocities are plotted relative to the *1D* model illustrated in Figure 3d. The dashed black line is drawn on the basis of the checkerboard test shown in Figure S7 and delimits the well resolved region. These maps show that the low-velocity anomalies *L1*, *L2* and *L3* extend throughout the upper mantle and below the *MTZ,* whereas *L4* and *L5* remain mostly confined to the upper mantle and surround the curved high-velocity body *H1*.

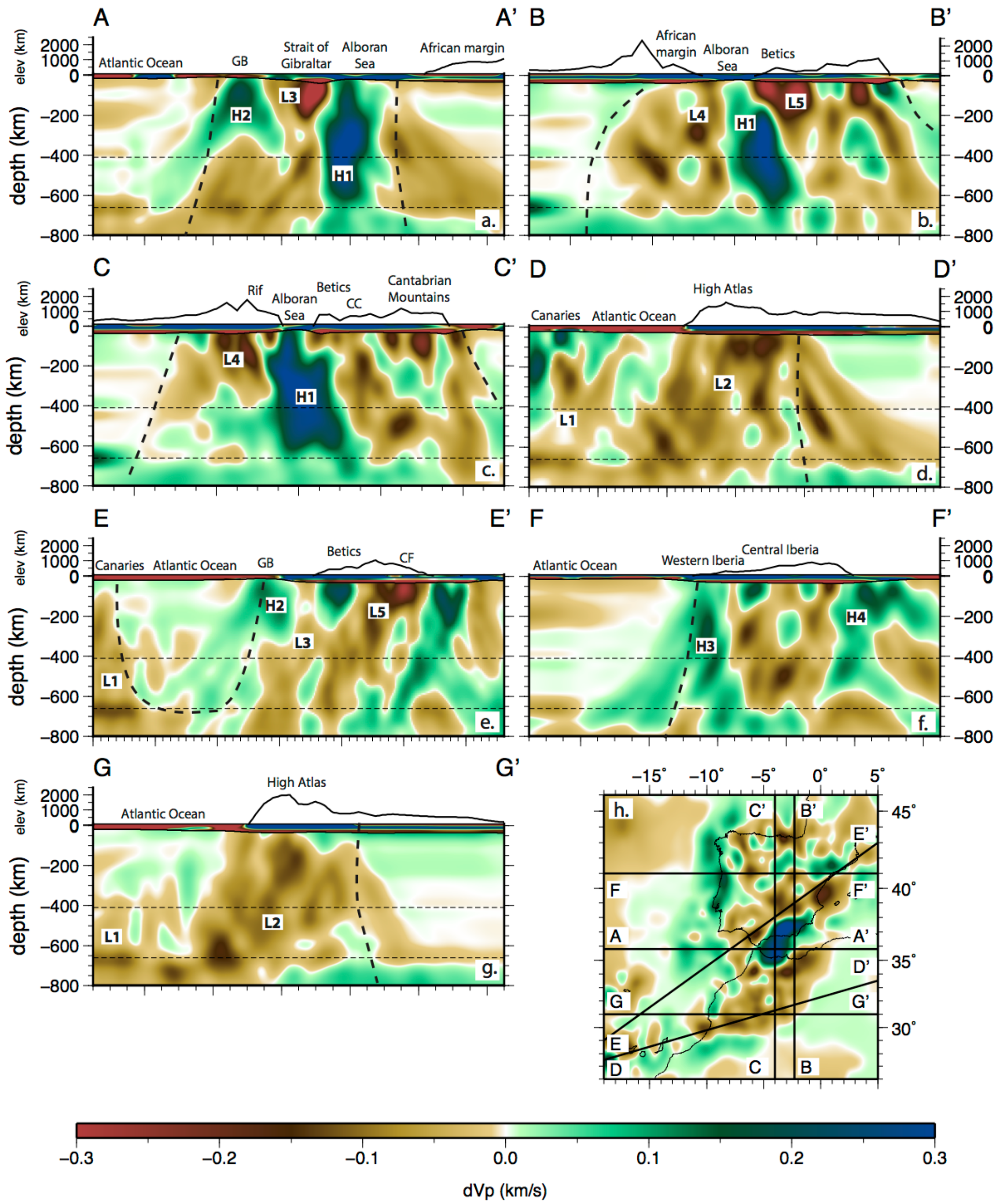

Figure 7. Vertical cross-sections through our *P*-wave model (damping = 5, smoothing = 5). Locations of the profiles are indicated with black lines in the 250 km depth slice (h). Topography profiles (from Smith and Sandwell, 1997) and geographic names are shown above each cross-section. Velocities are plotted relative to the *1D* model illustrated in Figure 3d. The thick dashed black line is drawn on the basis of the checkerboard test shown in Figure S7 and delimits the well resolved region. Relevant anomalies are identified in each profile. (a) Cross-section AA' cuts through subvertical mantle anomaly *L3* and through high-velocity bodies *H1* and *H2* below the Gorringe Bank and Alboran Sea. (b, c) BB' and CC' are cross-sections through *H1* and through low-velocity anomalies *L4* and *L5*. (d) Section DD' cuts the tilted structure *L1* below the Canaries and *L2* below the High Atlas. Note the width and continuity of *L2* from near the surface to *MTZ* depths. (e) Cross-section EE' cuts the *L1* and *L3* deep upwellings, *H2* and the *L5* upwelling. (f) Section FF' provides a view of the high-velocity anomalies *H3* and *H4*. (g) GG' is a cross-section through the northern part of the *L1* anomaly and the *L2* features. This profile shows the connection between *L1* and *L3* below the *MTZ*. We focus our attention on anomalies deeper than 50 km, where crossing rays are more abundant.

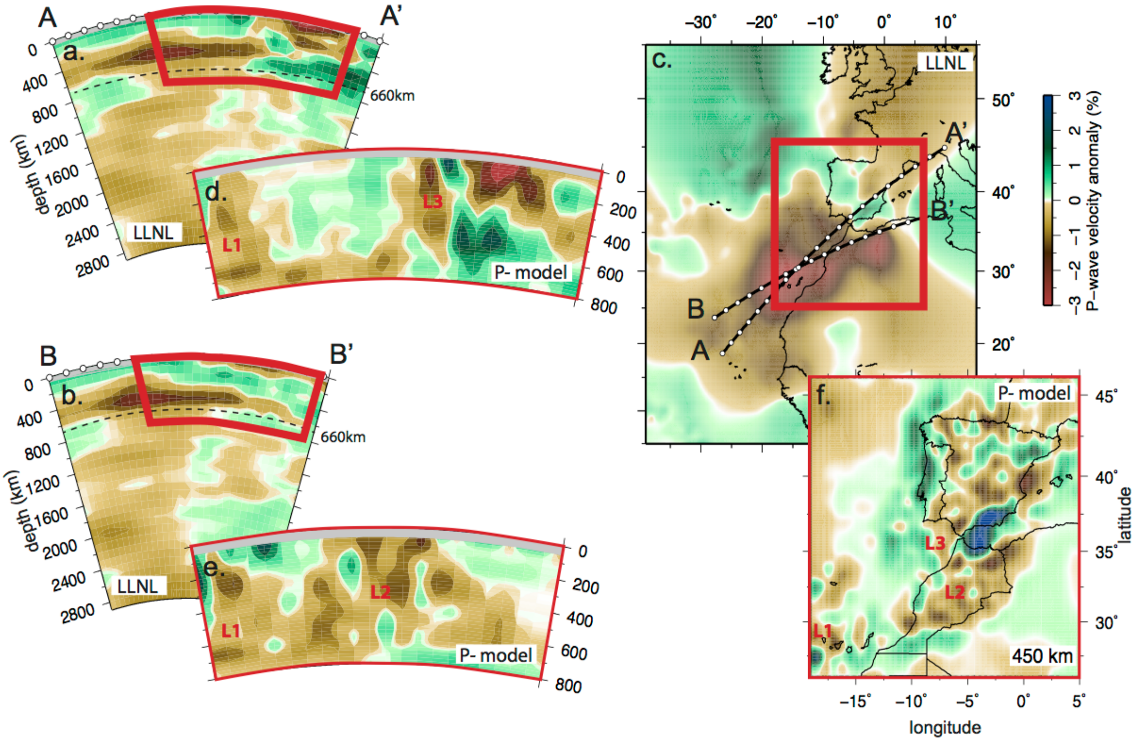

Figure 8. Comparison of global tomographic model *LLNL* (Simmons et al., 2012) and our regional *P*-wave model. (a, b) Vertical cross-sections through *LLNL* model. Location of the two profiles is shown in map view (c). (c) 450 km depth slice through *LLNL* model. (d, e) Cross-sections through our *P*-wave model with the same orientation as on a and b, respectively. (f) 450 km depth slice through our *P*-wave model. The red boxes in a, b and c indicate the limits of the corresponding regional *P*-wave model (this study). White points indicate the distance every 2°. Names of low-velocity anomalies *L1-L3* are indicated in red. The high-resolution model of this study better resolves small-scale low-velocity anomalies compared to the large low-velocity structure observed in the *LLNL* model. These relatively small-scale low-velocity anomalies appear to be rooted in the broad lower-mantle low-velocity anomaly seen in the *LLNL* model. Note that we image sub-vertical low-velocity features that model *LLNL* is not able to resolve.

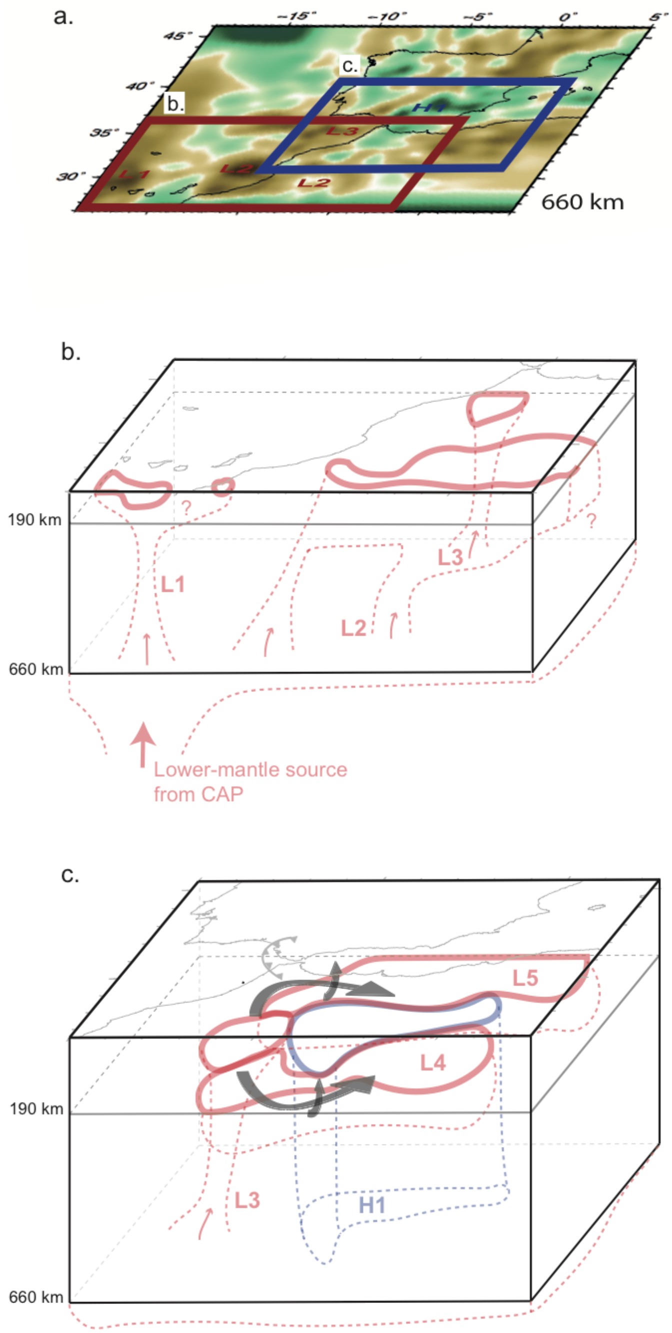

Figure 9. Schematic cartoon of the proposed geodynamical scenario based on our *P*-wave tomographic model. The two different mechanisms explaining the nature of the low-velocity features imaged are sketched separately in regions 9b and 9c. The thick red contours indicate the low-velocity anomalies; the thick blue contours represent the high-velocity anomaly. 190 km is the reference depth used to draw the low- and high-velocity features. The continuity of the anomalies at deeper depths has been drawn following their limits in the depth slices of Figure 6. (a) Map view through our *P*-wave model showing the location of regions b and c with red and blue boxes respectively. (b) Region including the Canaries, western Morocco and the southern part of the Gibraltar Arc system. We interpret the low-velocity structures *L1*, *L2* and *L3* we image through the *MTZ* as small-scale mantle upwellings fed by a lower-mantle source of hot material likely coming from *CAP*. (c) Region including the Gibraltar Arc System. We suggest that quasi-toroidal mantle flow induced by the retreating Gibraltar slab (*H1)* pushes material from mantle upwelling *L3* towards its lateral slab edges where the low-velocity anomalies *L4* and *L5* are found. Note that the lateral component of the subduction-induced quasi-toroidal flow is shown by large black arrows and the upward component is shown by small black arrows.

Supplementary material for online publication only

Click here to download Supplementary material for online publication only: Supplementary_high_resolution.pdf